Single-cell immune profiling of atherosclerosis: from omics to therapeutics

Depuydt, M.A.C.

Citation

Depuydt, M. A. C. (2024, March 28). *Single-cell immune profiling of atherosclerosis: from omics to therapeutics*. Retrieved from https://hdl.handle.net/1887/3729855

Version:	Publisher's Version
License:	Licence agreement concerning inclusion of doctoral thesis in the Institutional Repository of the University of Leiden
Downloaded from:	https://hdl.handle.net/1887/3729855

Note: To cite this publication please use the final published version (if applicable).

Chapter 4

Single-cell T-cell Receptor sequencing of paired human atherosclerotic plaques and blood reveals autoimmune-like features of expanded effector T-cells

Nature Cardiovascular Research 2023; 2:112–125

Marie A.C. Depuydt[1*], Frank H. Schaftenaar[1*], Koen H.M. Prange[2], Arjan Boltjes[3], Esmeralda Hemme[1], Lucie Delfos[1], Jill de Mol[1], Maaike J.M. de Jong[1], Mireia N.A. Bernabé Kleijn[1], Judith A.H.M. Peeters[4], Lauren Goncalves[4], Anouk Wezel[4], Harm J. Smeets[4], Gert J. de Borst[5], Amanda C. Foks[1], Gerard Pasterkamp[3], Menno P.J. de Winther[2], Johan Kuiper[1], Ilze Bot[1#], Bram Slütter[1#]

1. Leiden Academic Centre for Drug Research, Division of Biotherapeutics, Leiden University, Einsteinweg 55, 2333 CC Leiden, The Netherlands
2. Amsterdam University Medical Centers – location University of Amsterdam, Experimental Vascular Biology, Department of Medical Biochemistry, Amsterdam Cardiovascular Sciences, Amsterdam Infection and Immunity, Meibergdreef 9, Amsterdam, The Netherlands
3. Central Diagnostic Laboratory, University Medical Center, Utrecht University, Heidelberglaan 100, Utrecht, The Netherlands
4. Department of Surgery, Haaglanden Medisch Centrum Westeinde, 2512 VA The Hague, The Netherlands
5. Department of Vascular Surgery, University Medical Centre Utrecht, Heidelberglaan 100, Utrecht, The Netherlands

[*]These authors contributed equally; [#]Shared last authors

Abstract

Atherosclerosis is a lipid-driven chronic inflammatory disease, however, whether it can be classified as an autoimmune disease remains unclear. Here we apply single-cell TCR sequencing (scTCRseq) on human carotid artery plaques and matched PBMC samples to assess the extent of TCR clonality and antigen specific activation within the various T-cell subsets. We observed the highest degree of plaque-specific clonal expansion in effector CD4$^+$ T-cells and these clonally expanded T-cells expressed genes such as *CD69*, *FOS* and *FOSB* indicative of recent TCR engagement suggesting antigen-specific stimulation. CellChat analysis suggested multiple potential interactions of these effector CD4$^+$ T-cells with foam cells. Finally, we integrated a published scTCRseq dataset of the autoimmune disease psoriatic arthritis and report various commonalities between the two diseases. In conclusion, our data suggest that atherosclerosis has an autoimmune component driven by autoreactive CD4$^+$ T-cells.

Main

Atherosclerosis is the major underlying pathology of acute cardiovascular events, such as myocardial infarction and stroke. It is characterized by accumulation of lipids and subsequent inflammation of the medium and large arteries. As low-density lipoprotein (LDL) particles are important instigators of atherosclerosis, cardiovascular disease (CVD) has primarily been treated as a lipid-driven disorder with a treatment focus on lowering LDL cholesterol levels. Nonetheless, inflammation plays a critical role in perpetuating the growth and instability of atherosclerotic lesions, highlighted by the success of recent clinical trials with anti-inflammatory agents.[1,2] Elucidating the dominant inflammatory pathways that drive atherosclerosis may therefore allow identification of new druggable targets independent of cholesterol lowering.

Single-cell RNA sequencing (scRNAseq) and mass cytometry have allowed detailed mapping of the leukocyte contents of atherosclerotic plaques.[3,4] These studies show that T-cells are the largest leukocyte population and show that the number of effector T-cells within the lesion associates with plaque instability. In combination with previous murine work, this suggests inflammatory processes inside the plaque are driven by T-cells and atherosclerosis could be considered an autoimmune like disease. In support of that, autoreactive (LDL-specific) CD4$^+$ T-cells have previously been reported in the human atherosclerotic lesions and have been identified in elevated levels in the circulation CVD patients.[5-7] Moreover, vaccination approaches aimed at the reduction of self-reactive T-cells or induction of regulatory T-cells (T_{regs}) have shown promise in murine models of atherosclerosis.[8,9] However, when self-reactive CD4$^+$ T-cells are indeed the culprit T-cells that propagate disease, clonal expansion and accumulation of these cells in the lesions is to be expected. Interestingly, recent work examining the T-cell Receptor (TCR) distribution in human coronary plaques showed primarily clonal expansion of CD8$^+$ T-cells inside the plaque and identified some of these TCRs to be specific for common viral antigens such as Influenza, Cytomegalovirus (CMV) and SARS-CoV2.[10] However, this work did not include patient-matched PBMC controls, rendering it impossible to assess whether the virus-specific CD8$^+$ T-cells were specifically enriched in the plaque and/or had recently undergone antigen-specific interactions.

Here we present an approach to identify the T-cell subsets that are specifically enriched in atherosclerotic lesions and whether these subsets underwent antigen-specific interaction in the plaque. We combine scRNAseq and single-cell TCR seq (scTCRseq) of human carotid plaques and matched PBMC samples. With this approach, we observe the highest degree of plaque-specific clonal expansion in both effector

$CD4^+$ T-cells and to a smaller extent in the T_{reg} population. By integrating the data from our patients with atherosclerosis with scTCRseq data from psoriatic arthritis patients, we show that atherosclerosis has major similarities with another prominent autoimmune disease. Thus, our data suggest that atherosclerosis is characterized by an autoimmune component driven by autoreactive $CD4^+$ T-cells.

Results

Signature of antigen-specific T-cell in atherosclerosis

Recent scRNAseq studies in human atherosclerosis have shown a prominent accumulation of T-cells in the plaque.[3,4] Yet, it remains unclear whether these T-cells are bystanders or whether they actively contribute to lesion progression through antigen-specific activation. To examine potential recent antigen encounter and activation, CD69 expression was measured on the surface of both PBMC and plaque T-cells using flow cytometry (Cohort 1; **Fig. 1a, Supplementary Table 1**). A significant increase in $CD69^+$ $CD4^+$ (PBMC: 0.82% ± 0.71, plaque: 51.45% ± 16.39; P-value <0.0001) and $CD8^+$ T-cells (PBMC: 4.95% ± 6.49, Plaque: 55.20% ± 19.40; P-value <0.0001) was observed in the plaque compared to PBMCs (**Fig. 1b, Extended Data Fig. 1a, b**). Since CD69 is known to rapidly upregulate after TCR/HLA engagement on T-cells[11], these data suggest that T-cells actively engage in TCR-specific interactions within the atherosclerotic plaque.

Yet, CD69 expression may also indicate the presence of resident memory T-cells or may be upregulated by exposure to type I Interferon (IFN).[12,13] To determine whether the elevated CD69 expression was due to antigen-specific interactions in the plaque, we aimed to assess whether these T cells were clonally expanded as well. We combined scRNAseq with scTCRseq on paired PBMCs and carotid artery plaques from 3 male patients (Cohort 2; **Supplementary Table 1**). The plaques were enzymatically digested and live $CD45^+$ cells were isolated by fluorescent-activated cell sorting (FACS) (**Extended Data Fig. 2a**). Both PBMC and plaque cells were stained for CD3, CD4, CD8 and CD14 on a protein level with feature barcoding to properly distinguish between myeloid and T-cell subsets on both RNA and protein level. All cells were subsequently processed with droplet-based single-cell 5′ RNA sequencing (10X Genomics) and sequenced (**Fig. 2a**). Unsupervised clustering revealed clusters comprised of T-cells, NK cells, myeloid cells and B cells, originating from both PBMC and plaque cells and with limited interpatient variability (**Extended Data Fig. 2b-e**). We did not further characterize all non T-cells as we specifically focused on characterizing T-cells to assess their clonal expansion in atherosclerosis. Therefore, all T-cells were selected based on both RNA and protein expression and subsequently unsupervised clustering was performed independent of the variable TCR genes to prevent clustering based on clonality (see **Online methods**). Subclustering of both PBMC and plaque T-cells revealed 13 distinct T-cell subsets (**Fig. 2b, c, Extended Data Fig 2f**). Within the T-cells we observed one memory (C0) and three naive (C1, C2 and C10) T-cell clusters based on different expression levels of *TCF7*, *LEF1*, *SELL* and *CCR7* (**Fig. 2b, d, Supplementary Table 2)**. Furthermore, three effector T-cell clusters were detected (C3, C4, C5) expressing a multitude of different cytotoxic genes, amongst others *GZMB*, *GZMK*, *GZMA* (**Fig. 2b, d, Supplementary Table 2**). A T_{reg} cluster was defined based on expression of *FOXP3*, *IL2RA* and *TIGIT* (C6; **Fig 2b, d, Supplementary Table 2**).[14] In addition, an exhausted T-cell cluster characterized by expression of *HAVCR2*, *PDCD1* and *TOX*[15,16] (C7; **Fig. 2b, d, Supplementary Table 2**), and two γδ-T-cell clusters expressing *TRGC1*, *TRGC2*, *TRDC* (C8, C9; **Fig. 2b, d, Supplementary Table 2**) were detected. Lastly, we observed two small clusters consisting of mast cells (C11; **Fig. 2b, Supplementary Table 2**) and mucosal-invariant T-cells (MAIT; C12; **Fig. 2b, d, Supplementary Table 2**).

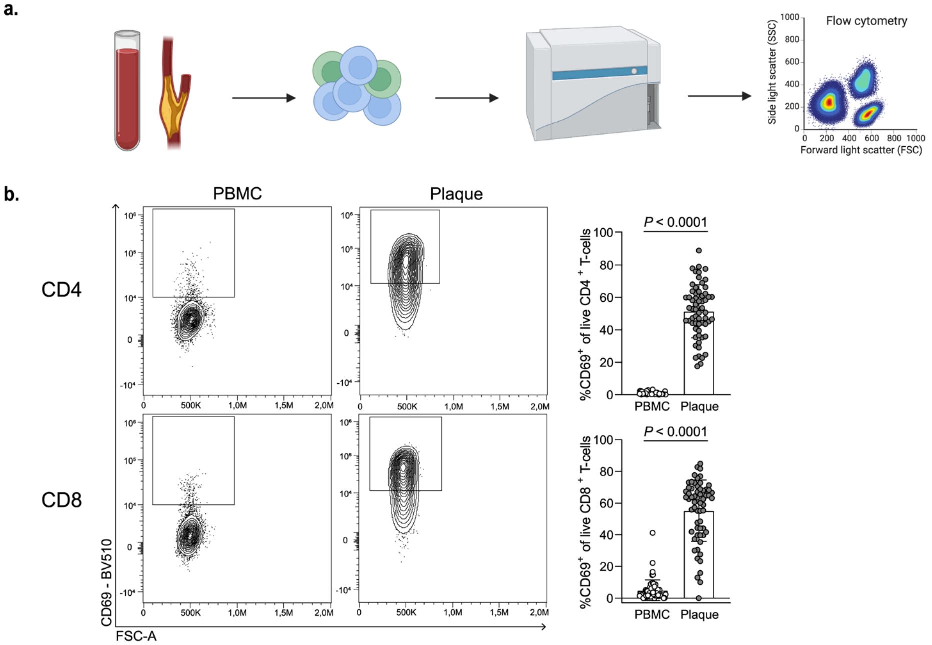

Fig. 1. Significant increase in $CD69^+$ T-cells in the atherosclerotic plaque suggests an antigen-specific T-cell response. a. Experimental set up: single cells from PBMC and plaque samples were stained with fluorescently labeled antibodies and measured with flow cytometry. **b.** Flow cytometry analysis of CD69 expression on PBMC and plaque live $CD4^+$ and $CD8^+$ T-cells. *P*-values are depicted in the figure panels. Data are presented as mean values ± SD. PBMC n = 58; plaque n = 61. Statistical analyses were performed using an unpaired Mann-Whitney T-test.

Next, we compared expression of *CD69*, as well as *FOS* and *FOSB*, genes which are also upregulated downstream of TCR signaling[17], between plaque and blood. In line with the increased CD69$^+$ protein expression measured with flow cytometry, all three genes showed an increased mRNA expression in plaque T-cells compared to their PBMC counterparts (**Fig. 2e**). Subsequently, we applied VDJ sequencing to map paired α- and β-chains of the TCR and to define the clonal composition of the paired PBMC and plaque T-cells. Clonal expansion levels were calculated to indicate the clonotype abundance as percentage of the total measured TCRs per patient per tissue (**Fig. 2f**, see **Online Methods**). 'Single' represents a single clonotype occurrence. Expanded T-cells were divided in multiple categories characterized by increasing frequencies of clonotype occurrences, labeled as respectively 'Small', 'Medium', 'Large' and 'Hyperexpanded'.

Fig. 2. Single-cell TCR sequencing reveals clonal expansion and antigen-specific activation of T-cells in the plaque. a. Schematic overview of the study design. Human plaques were enzymatically digested and live CD45$^+$ cells were sorted using fluorescent-activated cell sorting (FACS). Matched blood samples were processed to isolate PBMCs. Both plaque and PBMC cells were then further processed using 10X Genomics and sequenced. **b.** UMAP depicting 13 distinct T-cell clusters resulting from unsupervised clustering (n = 24443). **c.** UMAP showing contribution of PBMC or plaque to the T-cell clusters. **d.** Heatmap with average expression of T-cell function-associated genes. **e.** Violin plot with expression of *CD69*, *FOS* and *FOSB* in PBMC and plaque T-cells. **f.** UMAP visualization of clonotype expansion levels among T-cells between PBMC and plaque. **g.** Barplot with quantification of clonal expansion levels between plaque and PBMC T-cells. **h.** Barplot with quantification of tissue enrichment scores of clonotypes. **i.** Circle plots depicting tissue-enrichment scores of all T-cells per tissue and per patient. **j.** Barplot with quantification of clonal expansion levels between PBMC and plaque T-cells of bulk TCR-sequencing data (Cohort 3, n = 10). **k.** Barplot with quantification of Tissue enrichment scores of bulk TCR-sequencing data (Cohort 3). Clonotype expansion levels: Single (1 occurrence), Medium (>0.1 & ≤1%), Large (>1 & ≤10%), Hyperexpanded (>10%), percentage of all T-cells. Tissue enrichment scores: Plaque-enriched (Frequency expanded clone higher in Plaque vs. PBMC), Single (1 occurrence), Unenriched (Frequency expanded clone similar in PBMC vs. Plaque), PBMC-enriched (Frequency expanded clone higher in PBMC vs Plaque). ►

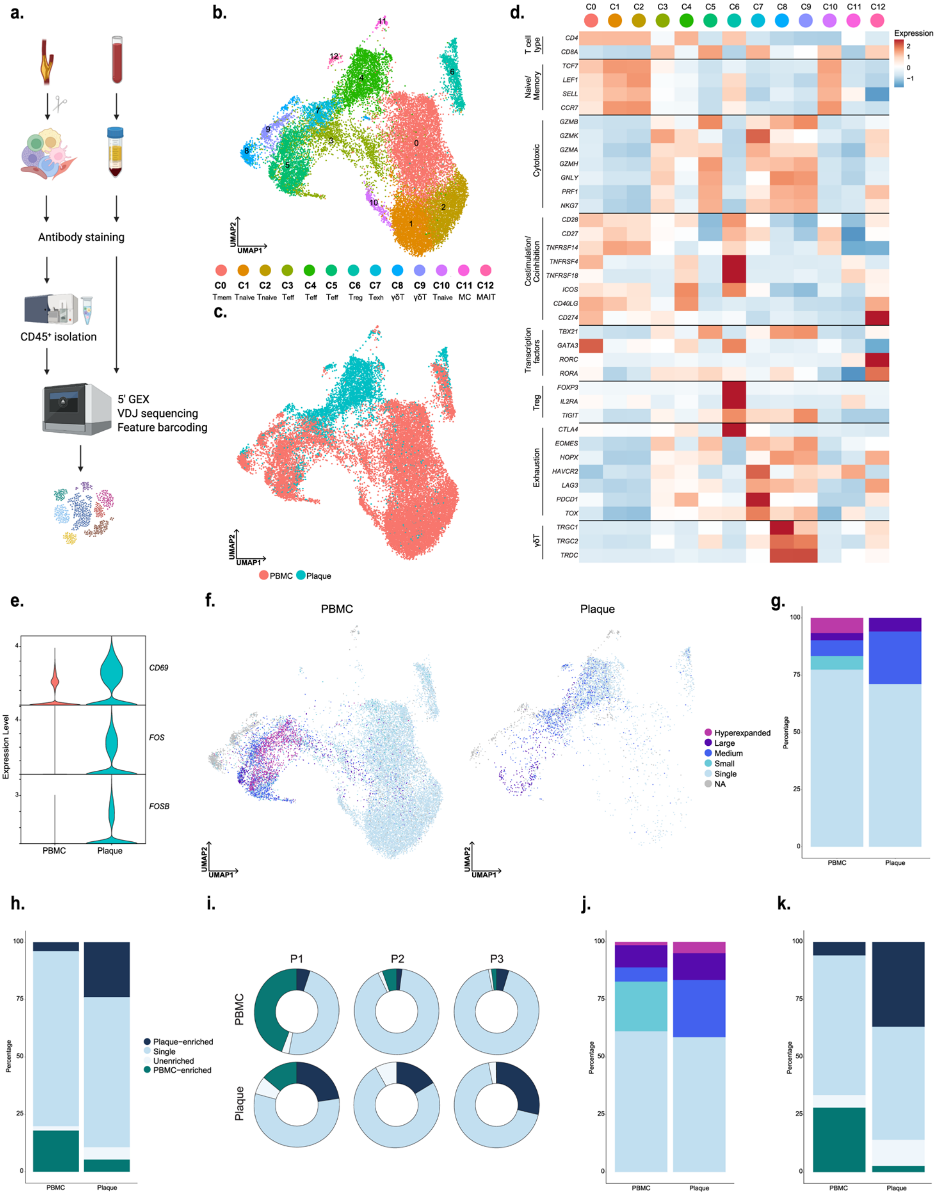
a.
Antibody staining
CD45+ isolation
5' GEX
VDJ sequencing
Feature barcoding
b.
UMAP2
UMAP1
C0 Tmem
C1 Tnaive
C2 Tnaive
C3 Teff
C4 Teff
C5 Teff
C6 Treg
C7 Texh
C8 γδT
C9 γδT
C10 Tnaive
C11 MC
C12 MAIT
c.
PBMC
Plaque
d.
C0 C1 C2 C3 C4 C5 C6 C7 C8 C9 C10 C11 C12
Expression
2
1
0
−1
T cell type
CD4
CD8A
Naive/Memory
TCF7
LEF1
SELL
CCR7
Cytotoxic
GZMB
GZMK
GZMA
GZMH
GNLY
PRF1
NKG7
Costimulation/Coinhibition
CD28
CD27
TNFRSF14
TNFRSF4
TNFRSF18
ICOS
CD40LG
CD274
Transcription factors
TBX21
GATA3
RORC
RORA
Treg
FOXP3
IL2RA
TIGIT
CTLA4
Exhaustion
EOMES
HOPX
HAVCR2
LAG3
PDCD1
TOX
γδT
TRGC1
TRGC2
TRDC
e.
Expression Level
CD69
FOS
FOSB
PBMC
Plaque
f.
PBMC
Plaque
Hyperexpanded
Large
Medium
Small
Single
NA
g.
Percentage
100
75
50
25
0
PBMC
Plaque
h.
Plaque−enriched
Single
Unenriched
PBMC−enriched
i.
P1
P2
P3
PBMC
Plaque
j.
k.

Taken together, a small increase in the percentage of total expanded T-cells is observed in the plaque compared to PBMCs (PBMC 23% vs. Plaque 29%; **Fig. 2f, g, Extended Data Fig. 3a, b, c, Supplementary Table 3**). One clonotype, originating from patient 1, was defined as hyperexpanded in the PBMC and large in the plaque. The TCRα-sequence of this clonotype matched with a TCRα-sequence previously associated with CMV in the VDJdb database (https://vdjdb.cdr3.net/).[18] The CD8$^+$ T-cell specific clonotype, however, was only expressed on T-cells that had little expression of *CD69*, *FOS* and *FOSB*, suggesting that this was not an active viral infection (**Extended Data Fig. 4a-c**). In addition, the tissue enrichment of clonotypes was assessed to investigate whether certain clonotypes specifically accumulated within either of the tissues, or whether the clonotype abundance was unaffected by the location. T-cells with clonotypes more present in the PBMC were identified as PBMC-enriched and vice versa for plaque-enriched T-cells. Indeed, within the plaque an increased percentage of plaque-enriched T-cells was observed in all patients, suggesting a potential plaque-restricted antigen-induced clonal expansion (**Fig. 2h, i, Extended Data Fig. 3d, e, Supplementary Table 3**). To confirm these findings, bulk TCRβ sequencing was performed on matched blood and plaque T-cells from 10 patients (Cohort 3; **Supplementary Table 1**). Both clonal expansion levels as well as tissue-enrichment were comparable between TCRβ bulk sequencing and the scTCRseq data (**Fig. 2j, k, Extended data Fig. 5a**).

Increased percentage of expanded CD8$^+$ T-cells in PBMCs

In order to properly isolate CD4$^+$ and CD8$^+$ T-cells for further analysis, a selection was made of CD4$^+$ and CD8$^+$ single positive T-cells based on expression of these proteins as measured by feature barcoding (**Extended Data Fig. 6a**). Subclustering of CD8$^+$ T-cells resulted in 11 distinct subsets. The majority of the CD8$^+$ T-cells had an activated phenotype as indicated by expression of multiple genes with a cytotoxic signature. One naive (C6) and one memory (C2) cluster were mainly detected in the PBMC (*TCF7*, *LEF1*, *SELL*, *CCR7*; **Fig. 3a, Extended Data Fig. 6b, c, Supplementary Table 2**). Four effector clusters were characterized of which C0 and C10 mostly reside in PBMC and C3 and C5 predominantly in plaque. C0, C3 and C10 expressed a multitude of different cytotoxic genes, including *GZMK* and *GZMA*, at different levels. C5 was characterized by expression of *CD69*, *FOS*, *FOSB* (**Fig. 3a, Extended Data Fig. 6b, c, Supplementary Table 2**). Furthermore, three terminally differentiated effector memory T-cell (T_{EMRA}) clusters were defined by expression of e.g. *GZMB*, *PRF1*, *NKG7* and lack of *CD27* and *CD28* (C1, C4, C7; **Fig. 3a, Extended Data Fig. 6b, c, Supplementary Table 2**). T_{EMRA} clusters were primarily associated with a gradual increase in expression of amongst others *KLRD1, KLRG1* and *FCGR3A*, indicating various stages of terminal differentiation (**Extended Data Fig. 6d**). Using Seurat multimodal reference mapping, which maps your data set to a large PBMC data set with feature barcoding data, expression of CD45RA and CD45RO could be predicted. Indeed, T_{EMRA} subsets were predicted to express CD45RA, whereas the effector T-cells were predicted to be CD45RO$^+$ (**Extended Data Fig. 6e**). Finally, a cluster of γδ-T-cells (C8) and a cluster of MAIT (C9) were detected within the CD8$^+$ T-cell subsets (**Fig. 3a, Extended Data Fig. 6a, b, Supplementary Table 2**). Subsequently, clonal expansion levels were examined and quantified within the CD8$^+$ T-cells in PBMC and plaque. A large percentage of clonally expanded CD8$^+$ T-cells was detected in the plaque, however a higher percentage of expanded CD8$^+$ T-cells was detected in the PBMC (**Fig. 3b, c, Extended Data Fig. 6f, Supplementary Table 3**). Nevertheless, within the plaque, the majority of the expanded CD8$^+$ T-cells remained plaque-enriched (**Fig. 3d, Extended Data Fig. 6g, Supplementary Table 3**). Expanded CD8$^+$ T-cells showed upregulation of multiple genes involved in CD8 cytotoxicity, eg. *GZMH*, *KLRD1*, *PRF1*, *GZMB* (**Fig. 3e**). Interestingly, when comparing PBMC-enriched versus plaque-enriched CD8$^+$ T-cells, PBMC-enriched cells expressed cytotoxic genes such as *GNLY*, *PRF1* and members of the killer cell lectin-like subfamily (*KLRG1*, *KLRD1*), whereas plaque-enriched CD8$^+$ T-cells seemed to have experienced recent antigen-induced TCR activation (**Fig. 3f**). To further illustrate the plaque-expanded CD8$^+$ T-cell clusters, we selected C1, C3, C5 and C9 which had relatively the most plaque-enriched expansion (**Fig. 3g**). C1, C3 and C5 all expressed a multitude of cytotoxic genes. C1 highly expressed *NKG7*, *GNLY* and *GZMB*, of which the latter was increased in plaque, whereas C3 and C5 had increased expression of *GZMA* and *GZMK* in the plaque. C5 plaque T-cells had the highest expression of *CD69*, *FOS* and *FOSB*. Finally, MAIT-cells (C9) showed high expression of genes unique for this cell type (*TRAV1-2*, *ZBTB16*, *IL23R*)[19] and of TCR activation genes. To identify potential dynamics of different CD8$^+$ populations, we applied lineage tracing analyses using Monocle3 and RNA velocity. RNA velocity shows that within the CD8$^+$ clusters, cells tend to be less prone to switch into another subset. A small trajectory appeared between the memory CD8$^+$ T-cells (C2) and the antigen-experienced effector T-cells (C5), yet this was not clearly retrieved with pseudotime analysis (**Fig. 3i, j**).

Increased percentage of expanded CD4$^+$ T-cells in plaque

Unsupervised clustering revealed 11 subsets of CD4$^+$ T-cells (**Fig. 4a**). As previously described, CD4$^+$ T-cell clusters are mainly defined by a shift in activation status.[3,4] Two naive T-cell clusters (C1, C2) and a memory T-cell cluster (C0) were mainly detected within the PBMC (**Fig. 4a, Extended Data Fig. 7a, b, Supplementary Table 2**). Furthermore, a T-helper (T_h) 17-like cluster (C4) expressing *RORC*, *RORA* and *CCR6* as well as a T_{reg} cluster (C5; **Fig 4a, Extended Data Fig. 7b, Supplementary Table 2**) were identified. Whereas T_{regs} were found in both PBMC and plaque, T_{h17}-like cells were mainly detected in PBMCs (**Extended Data Fig. 7c**). A T-cell cluster with genes involved in cell migration (T_{migr}, C6) mainly resided in PBMCs (**Supplementary Table 2**). Two different effector subsets were characterized, of which one more plaque-specific with high expression of *CD69*, *FOS*, *JUN* and *GZMA* (C3) and one found in both tissues specifically enriched for *GZMK* (C8; **Fig. 4a, Extended Data Fig. 7a, b, Supplementary Table 2**). Moreover, a cytotoxic CD4$^+$ T-cell cluster, that resembled the previously described CD4$^+$CD28^{null} cells[3,20,21], was defined by expression of *GZMB*, *PRF1* and lack of *CD28* and was found in both PBMC and plaque (**Fig. 4a, Extended Data Fig. 6a, b, Supplementary Table 2**). Finally, a cluster of T-cells was observed in the PBMCs that expressed genes involved in IFN I signaling and a small mast cell cluster in the plaque (**Fig. 4a**, **Supplementary Table 2**). Subsequently, CD4$^+$ T-cell clonality was assessed. Clonal expansion levels were projected on the CD4$^+$ T-cell UMAP and quantified. In line with a recent study by Chowdhury *et al.*[10], the percentage of clonal expanded CD8$^+$ T-cells in the plaque is larger than those in CD4$^+$ T-cells. However, in contrast to CD8$^+$ T-cells, a marked increase in the percentage of expanded CD4$^+$ T-cells in the plaque was revealed compared to the PBMCs (**Fig. 4b, c, Extended Data Fig. 7e, Supplementary Table 3**). Furthermore, the expanded clonotypes in the plaque CD4$^+$ T-cells were mostly plaque-enriched (**Fig. 4d, Extended Data Fig. 7f, Supplementary Table 3**). When comparing expanded CD4$^+$ T-cells to their single counterparts with a unique clonotype, upregulation of genes involved in T-cell activation and cytotoxicity, such as *GNLY*, *GZMH*, *PRF1*, *CX3CR1*, were particularly observed in the expanded T-cells, whereas single T-cells expressed genes upregulated in naive and memory T-cells (*CCR7*, *LTB*, *LEF1*, *SELL*, *CD27*)(**Fig. 4e**). Interestingly, when comparing clonally expanded PBMC-enriched versus the plaque-enriched expanded CD4$^+$ T-cells, plaque-enriched CD4$^+$ T-cells showed enhanced expression of genes upregulated shortly after antigen-specific TCR interaction (*JUN*, *CD69*, *FOS*, *FOSB*) (**Fig. 4f**), suggesting there are CD4$^+$ T-cells that undergo antigen-specific interactions in the plaque. Next, we quantified the absolute number of plaque-enriched clones per CD4$^+$ T-cell cluster (**Fig. 4g**), which revealed cluster C3 as the major contributor in absolute number of plaque-specific clonally expanded T-cells. Furthermore, C7 and C8 consisted of a relatively large number of plaque-enriched clones compared to the other CD4$^+$ T-cell clusters. The C7 cluster, characterized by an increase in cytotoxic genes, including *GZMB*, *NKG7* and *PRF1*, has little to no expression of *CD69*, *FOS*, *FOSB*, indicating that although these cells have significant expanded clonotypes, they do not express genes involved in antigen-induced activation (**Fig. 4h**). The effector populations C3 and C8 displayed increased expression of TCR proximal genes *CD69*, *FOS* and *FOSB*. Interestingly, whereas we did not observe increased accumulation of clonally expanded T$_{regs}$ (C5) in plaque, we did observe upregulation of *FOS*, *FOSB* and *JUN* in plaque-derived T$_{regs}$ compared to PBMC-derived T$_{regs}$, suggesting T$_{regs}$ are encountering antigen in the plaque. Expression of various functional T$_{reg}$ markers (*FOXP3*, *IL2RA*, *TIGIT*, *CTLA4*, *TNFRSF4* (OX40) and *TNFRSF18* (GITR)) in the plaque compared to the PBMC, indicated increased activity of T$_{regs}$ (**Fig. 4h, 4i**).

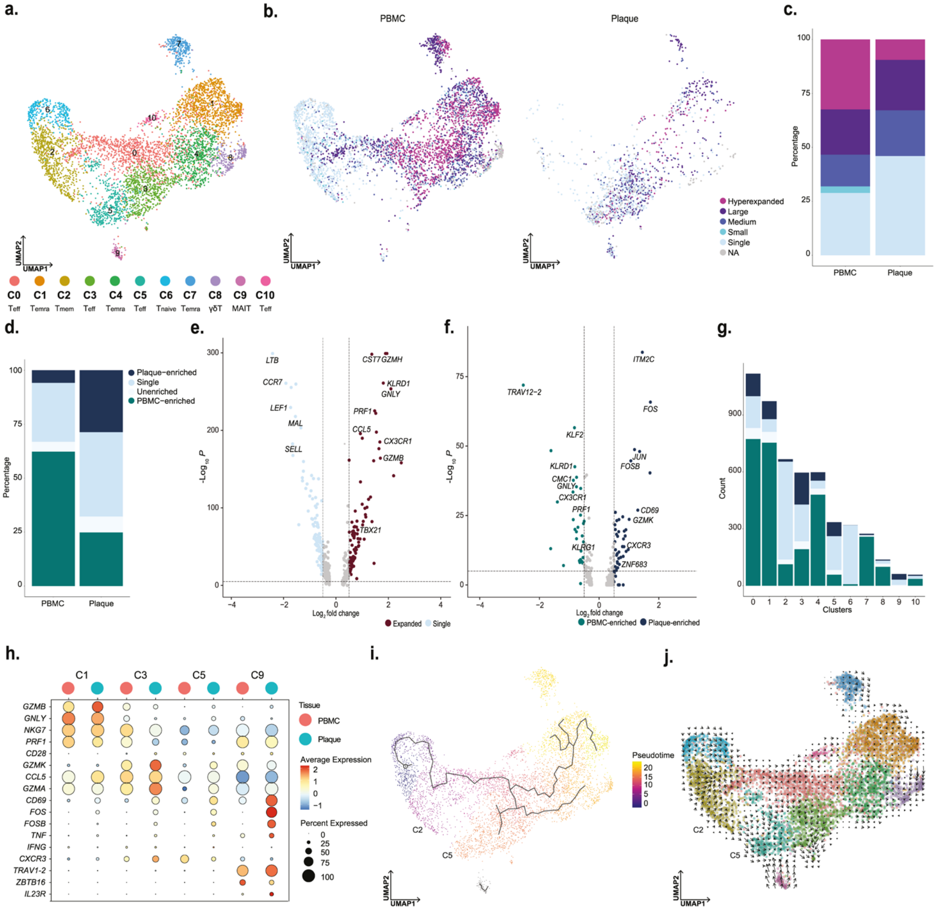

◄ **Fig. 3. Limited clonal expansion in plaque CD8⁺ T-cells compared to PBMC. a.** UMAP visualization of unsupervised clustering revealed 11 distinct CD8⁺ T-cell populations (n = 5730). **b.** UMAP visualization of different levels of clonotype expansion among CD8⁺ T-cells between PBMC and plaque. **c.** Quantification of clonal expansion levels between PBMC and plaque CD8⁺ T-cells. **d.** Quantification of tissue enrichment scores of clonotypes in CD8⁺ T-cells of PBMC and plaque. **e.** Volcano plot with differentially expressed genes between CD8⁺ T-cells with Single clonotypes and all expanded clonotypes (Small-Large). Genes were considered significant with a *P*-value $< 10e^{-6}$ and a fold change of 0.5. For all Volcano plots, Bonferroni corrected *P*-values were calculated based on the total number of genes in the dataset. **f.** Volcano plot with differentially expressed genes of PBMC-enriched versus plaque-enriched CD8⁺ T-cells. Genes were considered significant with a *P*-value $< 10e^{-6}$ and a fold change of 0.5. **g.** Barplot with quantification of tissue-enrichment score of individual CD8⁺ T-cell clusters. **h.** Dotplot of average expression of upregulated genes in cluster 1, 3, 5 and 9. **i.** UMAP visualization of pseudotime analysis of CD8⁺ T-cells. C2 indicates cluster 2; C5 indicates cluster 5. **j.** UMAP visualization of RNA velocity analysis of CD8⁺ T-cells. Clonotype expansion levels: Single (1 occurrence), Medium (>0.1 & ≤1%), Large (>1 & ≤10%), Hyperexpanded (>10%), percentage of all CD8⁺ T-cells. Tissue enrichment scores: Plaque-enriched (Frequency expanded clone higher in Plaque vs. PBMC), Single (1 occurrence), Unenriched (Frequency expanded clone similar in PBMC vs. Plaque), PBMC-enriched (Frequency expanded clone higher in PBMC vs Plaque).

Fig. 4. Increased percentage of expanded and plaque-enriched CD4⁺ T-cells in the atherosclerotic plaque. a . UMAP visualization of unsupervised clustering revealed 11 distinct CD4⁺ T-cell populations (n = 17073). **b.** UMAP visualization of different levels of clonotype expansion among CD4⁺ T-cells between PBMC and plaque. **c.** Barplot with quantification of clonal expansion levels between PBMC and plaque CD4⁺ T-cells. **d.** Barplot with quantification of tissue enrichment scores of clonotypes in CD4⁺ T-cells of PBMC and plaque. **d.** Volcano plot with differentially expressed genes between CD4⁺ T-cells with Single clonotypes and all expanded clonotypes (Small-Large). Genes were considered significant with a *P*-value $< 10e^{-6}$ and a fold change of 0.5. For all Volcano plots, Bonferroni corrected *P*-values were calculated based on the total number of genes in the dataset. **f.** Volcano plot with differentially expressed genes of PBMC-enriched versus plaque-enriched CD4⁺ T-cells. Genes were considered significant with a *P*-value $< 10e^{-6}$ and a fold change of 0.5. **g.** Barplot with quantification of tissue-enrichment score of individual CD4⁺ T-cell clusters. **h.** Dotplot of average expression of upregulated genes in cluster 3, 5, 7 and 8. **i.** Volcano plot with differentially expressed genes between regulatory T-cells in PBMC and plaque. Genes were considered significant with a *P*-value $< 10e^{-6}$ and a fold change of 0.5. **j.** UMAP visualization of pseudotime analysis of CD4⁺ T-cells. Two branches of the analysis have been indicated with 1 and 2.**k.** UMAP visualization of RNA velocity analysis of CD4⁺ T-cells with close-up of branch 1 and 2. **l.** UMAP visualization of four overlapping clonotypes between cluster 6 and cluster 3. Open circles indicate PBMC CD4⁺ T-cells, closed circles indicate plaque CD4⁺ T-cells. Clonotype expansion levels: Single (1 occurrence), Medium (>0.1 & ≤1%), Large (>1 & ≤10%), percentage of all CD4⁺ T-cells. Tissue enrichment scores: Plaque-enriched (Frequency expanded clone higher in Plaque vs. PBMC), Single (1 occurrence), Unenriched (Frequency expanded clone similar in PBMC vs. Plaque), PBMC-enriched (Frequency expanded clone higher in PBMC vs Plaque). ►

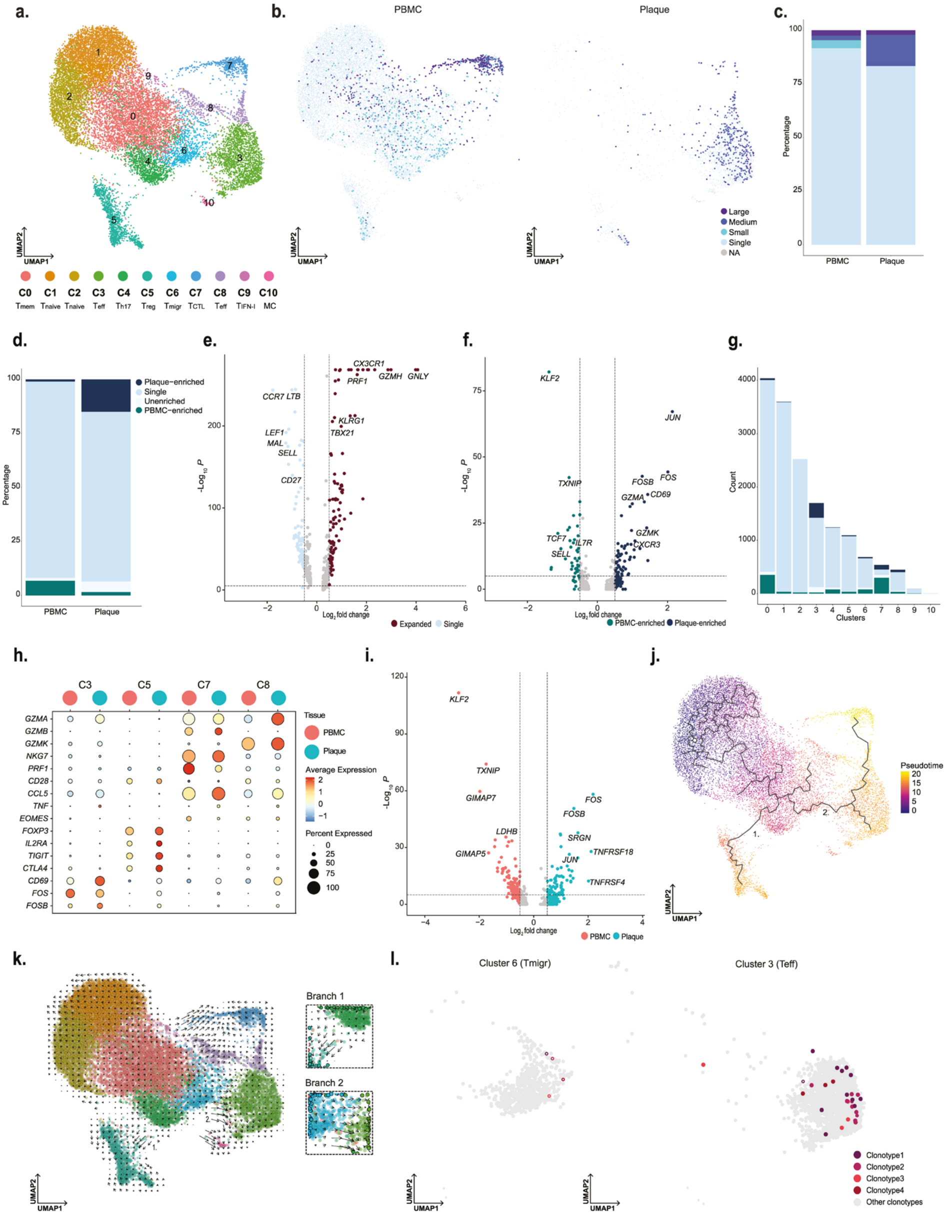
a.
b.
PBMC
Plaque
c.
Large
Medium
Small
Single
NA
Percentage
PBMC
Plaque
UMAP1
UMAP2
C0 Tmem
C1 Tnaive
C2 Tnaive
C3 Teff
C4 Th17
C5 Treg
C6 Tmigr
C7 TCTL
C8 Teff
C9 TIFN-I
C10 MC
d.
Plaque−enriched
Single
Unenriched
PBMC−enriched
e.
CX3CR1
GZMH
GNLY
PRF1
CCR7 LTB
LEF1
MAL
SELL
KLRG1
TBX21
CD27
Log2 fold change
-Log10 P
Expanded
Single
f.
KLF2
JUN
TXNIP
FOSB
FOS
GZMA
CD69
TCF7
IL7R
SELL
GZMK
CXCR3
PBMC-enriched
Plaque-enriched
g.
Count
Clusters
h.
C3
C5
C7
C8
GZMA
GZMB
GZMK
NKG7
PRF1
CD28
CCL5
TNF
EOMES
FOXP3
IL2RA
TIGIT
CTLA4
CD69
FOS
FOSB
Tissue
PBMC
Plaque
Average Expression
Percent Expressed
i.
KLF2
TXNIP
GIMAP7
LDHB
GIMAP5
FOS
FOSB
SRGN
TNFRSF18
JUN
TNFRSF4
PBMC
Plaque
j.
Pseudotime
k.
Branch 1
Branch 2
l.
Cluster 6 (Tmigr)
Cluster 3 (Teff)
Clonotype1
Clonotype2
Clonotype3
Clonotype4
Other clonotypes

To identify the origin of the antigen-specific effector CD4$^+$ T-cell subsets in the plaque, we applied lineage tracing analyses to define the dynamics of the different CD4$^+$ T-cell populations. Pseudotime analysis using Monocle3 showed a trajectory ranging from naive T-cells towards either the T_{regs} (Branch 1) or towards the effector T-cell population (Branch 2; **Fig. 4j**). The first pseudotime branch directing towards T_{regs} is projected through the T_{h17}-like CD4$^+$ T-cell cluster, potentially suggesting a plasticity between both subtypes. Yet, if the complementary RNA velocity analysis is assessed (time-resolved analysis based on spliced and unspliced mRNA[22]), the T_{reg} cluster does not seem to be derived from the T_{h17}-like cells (Branch 1; **Fig. 4k**). Moreover, T_{regs} in tissue also cluster further away from the circulating T_{h17}-like cells compared to the PBMC T_{regs}, indicating that the plaque environment is less likely to induce a phenotype switch from T_{regs} to T_{h17}. In addition, no overlapping clonotypes were found between both clusters and *FOXP3* and *RORC* did not co-express (**Extended Data Fig. 7b, c**), suggesting that in our data set we were not able to detect the previously described T_{reg}/T_{h17} plasticity.[23] Looking at the other branch in both pseudotime analysis and RNA velocity (Branch 2), a clear path ranging from the T_{migr} cluster (C6) towards the CD69$^+$ T_{eff} cluster (C3) is observed. Their migratory phenotype, highlighted by expression of *CCR4* and *CCR10* previously described to be expressed on infiltrating T-cells in the inflamed skin[24], suggests that this T_{migr} subset could be the precursor population for the antigen-specific CD4$^+$ T-cells in the plaque (**Extended Data Fig. 7d**). Indeed, when comparing overlap in TCR sequence between the different CD4$^+$ subpopulations, 37 clonotypes overlapped between both cluster C6 and C3. Within the top 5 most expanded clonotypes, 4 plaque-enriched clonotypes were detected and exhibited marked expansion in C3 compared to C6, further confirming our hypothesis that the clonally expanded T_{eff} cells could originate from the circulating migratory T-cell subset (**Fig. 4l, Extended Data Fig. 7c**).

TREM2$^+$ macrophages can activate antigen-induced CD4$^+$ T-cells

Our data suggests atherosclerotic plaques harbor one major CD4$^+$ T-cell subset that regularly undergoes antigen-specific interactions. To understand whether and how these clonally expanded T-cells interacted with myeloid subsets in the plaque, we selected five plaque myeloid cell populations from the overall data set: myeloid-derived dendritic cells (DC-M), plasmacytoid DCs (DC-P), proliferating macrophages (M-Prol), inflammatory macrophages (M-Inf) and foamy TREM2^{hi} macrophages (M-TREM2) (**Extended data Fig. 8a**).[3] Using CellChat we examined potential signaling pathways between these myeloid subsets and the CD4$^+$ and CD8$^+$ T-cells in the plaque.[25] CellChat can predict incoming (receptor), and outgoing (ligand) activity of cell-signaling pathways based on scRNA-seq data, accounting for the multimeric structure of ligand-receptor complexes, and the effect of co-factors on the ligand-receptor interactions. Predicted outgoing and incoming pathway signaling were displayed per cluster. Overlap between outgoing and incoming signals of a certain pathway within or between clusters, indicate a possible interaction through this pathway. The different CD4$^+$ T-cell clusters showed different levels of relative signaling strength in the outgoing signaling patterns (top barplot heatmap, relative to outgoing signals of all pathways in the heatmap), whereas CD8$^+$ T-cells showed little difference between the clusters (**Fig. 5a, Extended data Fig. 8b**). In general, the most upregulated signaling pathway was MHCII as outgoing signal on all myeloid subsets and incoming signals in multiple CD4$^+$ T-cell subsets, including cluster 3 (C3). The plaque-enriched CD69$^+$ C3 displayed elevated outgoing signaling patterns. Interestingly, one of the pathways that was enriched in this cluster, is the CD40 pathway, involved in antigen-specific T-cell activation.[26] Next, we assessed whether the CD40 pathway was also enriched as incoming signaling pattern (**Fig. 5b**). Specific enrichment was observed in the M-TREM2 (foam cell) subset. Apart from the CD40 pathway, multiple other enriched pathways involved in immune synapse formation and co-stimulation could be defined between C3 and M-TREM2, including the CD99, CD6, CD40, Macrophage Inhibitory Factor (MIF) and Annexin A1 pathways (**Fig. 5b**).[27-30] Together, this suggests that M-TREM2 could be involved in activation of the clonally expanded CD4$^+$ T-cells in atherosclerotic lesions.

Common autoimmune phenotype in expanded plaque T-cells

Based on the accumulation of plaque-enriched CD4$^+$ and CD8$^+$ T-cell clonotypes, we hypothesized that human atherosclerosis could be characterized as an autoimmune driven T-cell response. To further confirm this hypothesis, we integrated a scTCRseq data set of the autoimmune disease psoriatic arthritis (PSA), containing data from PBMC and synovial fluid (SF).[31] As in this study CD45RA$^-$ T-cells were isolated, we excluded the naive T-cell clusters from our data set. Moreover, this study did not include feature barcoding. CD4$^+$ and CD8$^+$ T-cells were therefore selected based on the labels predicted by multimodal reference mapping (**Extended Data Fig. 9a-f**). Subsequently, CD4$^+$ and CD8$^+$ T-cells of both diseases were integrated (**Extended Data Fig. 9g, h**) and projected on the atherosclerosis CD4$^+$ and CD8$^+$ UMAP as reference. Remarkably, a clear overlap between PBMCs from atherosclerosis and PSA was observed in both CD4$^+$ and CD8$^+$ T-cells. In addition, this overlap was also seen between plaque and SF for both T-cell subsets (**Fig. 6a, b**). Next, clonal expansion levels were recalculated for both atherosclerosis and PSA (percentage of all CD4$^+$ or CD8$^+$ detected TCRs). Indeed, clonally expanded T-cells were found in similar CD4$^+$ and CD8$^+$ T-cell clusters in both diseases (**Fig. 6c, e**). Moreover, quantification of this clonal expansion revealed a similar distribution. An increased percentage of expanded CD8$^+$ T-cells versus expanded CD4$^+$ T-cells was detected in SF. However, as seen in atherosclerosis, the percentage of expanded CD4$^+$ T-cells was increased in SF compared to PBMC, whereas expanded CD8$^+$ T-cells did not differ between both tissues (**Fig. 6d, f**). Tissue-enrichment scores were also determined and again displayed similarities between atherosclerosis and PSA. Tissue-enriched T-cells were located in overlapping clusters in both diseases. Quantification resulted in an increase in tissue-enriched T-cells in both CD4$^+$ and CD8$^+$ in plaque and SF compared to their matched PBMCs, although this enrichment was more prominent in SF versus plaque T-cells (**Fig. 6g-j**). Finally, we defined the genes supporting the overlap between the atherosclerosis and PSA subsets in C3 and C5 of both CD4$^+$ and CD8$^+$ T-cells. CD4$^+$ T-cells from C3 were characterized by high expression of *CCL5*, *GZMK* and *GZMA* in both plaque and SF (**Fig. 6k, Extended Data Fig. 10a**). Atherosclerosis-specific C3 CD4$^+$ T-cells had slightly increased *GZMA* expression compared to PSA PBMC and SF. In both diseases, *FOS* and *JUN* were upregulated in tissue compared to PBMC, whereas *FOSB* was specifically upregulated in plaque T-cells. Furthermore, regulatory CD4$^+$ T-cells in both affected tissues appeared more active by upregulation of activation markers, including *IL2RA*, *TNFRSF4*, *TNFRSF18*, *TNFSF1B* and *CTLA4*, compared to the PBMC counterpart (**Fig. 6l, Extended Data Fig. 10b**). Nevertheless the Treg subset showed some disparity between SF and plaque derived cells as plaque T_{regs} also increasingly expressed *ICOS* and *ENTPD1*, compared to PSA SF derived T_{regs}. Interestingly, atherosclerosis T_{regs} in both PBMC and plaque had increased expression of *TGFB1* compared to the PSA T_{regs}. In both PSA and atherosclerosis CD8$^+$ C3 T-cells, expression profiles displayed a comparable phenotype with high expression of T-cell effector genes, eg. *CCL5*, *GZMH*, *GZMA*, *GZMK* and *NKG7* (**Fig. 6m, Extended Data Fig. 10c**). Lastly, CD8$^+$ T-cells from C5 showed upregulation of genes involved in antigen-induced TCR activation in both affected tissues (*FOS*, *JUN*) (**Fig. 6n, Extended Data Fig. 10d**). *FOSB* was upregulated in plaque only, similar to CD4$^+$ C3 and *JUNB* expression was increased in PSA compared to atherosclerosis. Furthermore, increased expression of *ZNF683* was observed in both diseased tissues. *GZMH* was particularly upregulated in plaque CD8$^+$ T-cells. To summarize, these data support the hypothesis that atherosclerosis has a significant autoimmune component as it has phenotypically similar clonally expanded T-cells compared to the autoimmune disease PSA.

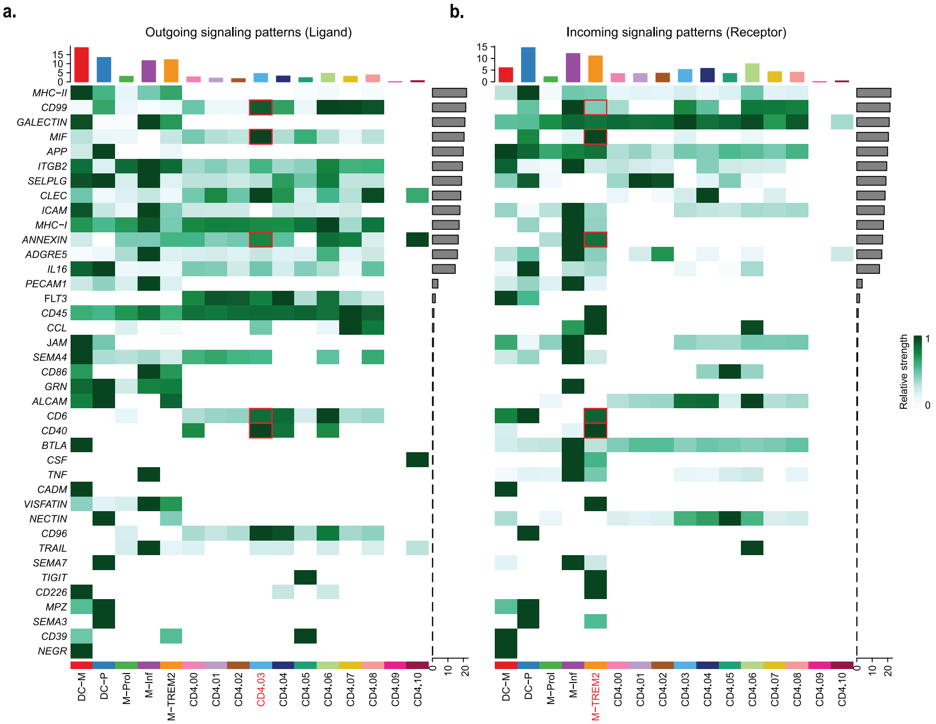

Fig. 5. Enriched interaction pathways between CD4$^+$ T$_{eff}$ cells and TREM^{hi} macrophages. a. Heatmaps displaying outgoing (Ligand) and **b.** incoming signaling (Receptor) patterns of pathways describing potential ligand-receptor interactions. Scale above heatmap indicates the relative signaling strength of a cell cluster based on all signaling pathways displayed in the heatmap. Grey bars right of the heatmap show the total signaling strength of a pathway in all cell clusters. The relative signaling strength indicated by ranging color from white (low) to green (high). DC-M indicates myeloid-derived dendritic cell (DC); DC-P indicates plasmacytoid DC; M-PROL indicates proliferating macrophages; M-Inf indicates inflammatory macrophage; M-TREM2 indicates TREM2^{hi} macrophages. All cells included in these graphs originate from the plaque.

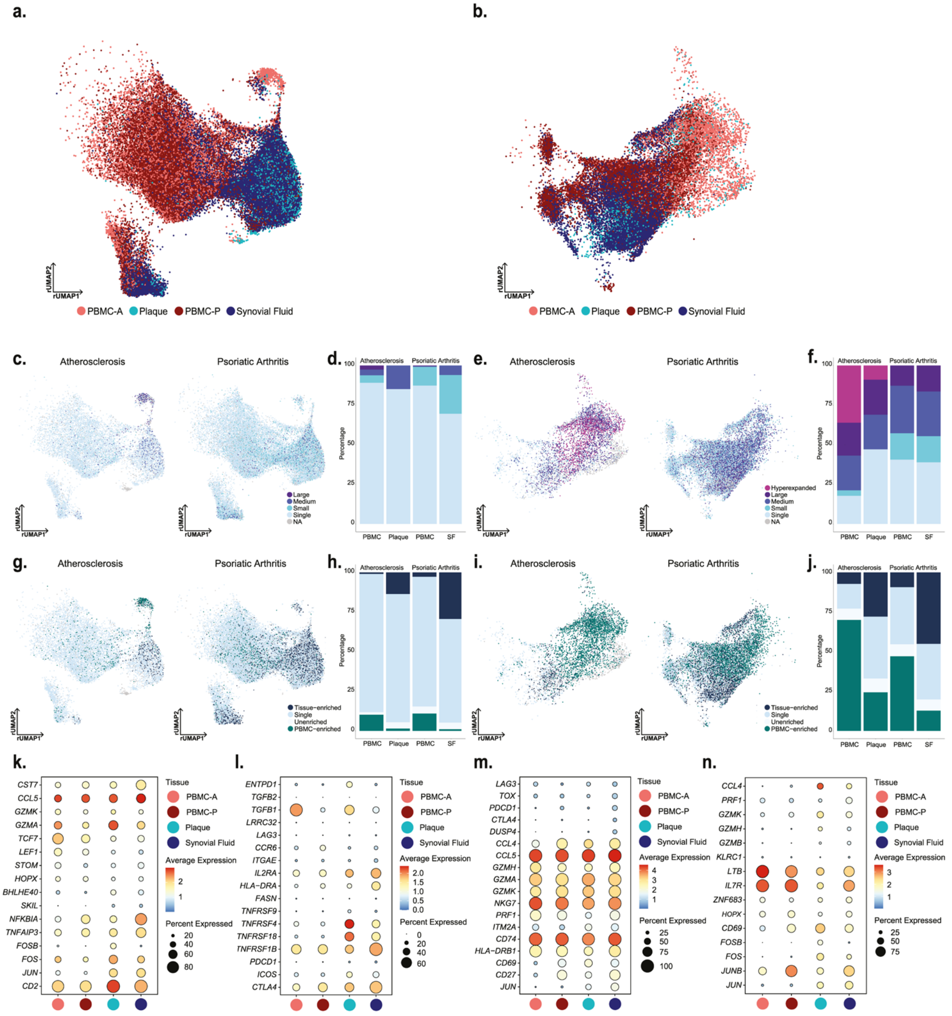
a.
b.
rUMAP1
rUMAP2
PBMC-A
Plaque
PBMC-P
Synovial Fluid
c.
Atherosclerosis
Psoriatic Arthritis
Large
Medium
Small
Single
NA
d.
Percentage
PBMC
Plaque
SF
e.
Hyperexpanded
f.
g.
Tissue−enriched
Unenriched
PBMC−enriched
h.
i.
j.
k.
CST7
CCL5
GZMK
GZMA
TCF7
LEF1
STOM
HOPX
BHLHE40
SKIL
NFKBIA
TNFAIP3
FOSB
FOS
JUN
CD2
Tissue
Average Expression
Percent Expressed
l.
ENTPD1
TGFB2
TGFB1
LRRC32
LAG3
CCR6
ITGAE
IL2RA
HLA−DRA
FASN
TNFRSF9
TNFRSF4
TNFRSF18
TNFRSF1B
PDCD1
ICOS
CTLA4
m.
LAG3
TOX
PDCD1
CTLA4
DUSP4
CCL4
CCL5
GZMH
GZMA
GZMK
NKG7
PRF1
ITM2A
CD74
HLA−DRB1
CD69
CD27
JUN
n.
CCL4
PRF1
GZMK
GZMH
GZMB
KLRC1
LTB
IL7R
ZNF683
HOPX
CD69
FOSB
FOS
JUNB
JUN

◂ **Fig. 6. Tissue-enriched clonal expanded CD4$^+$ and CD8$^+$ T-cells of atherosclerosis and psoriatic arthritis have phenotypic commonalities. a.** Atherosclerosis and psoriatic arthritis CD4$^+$ T-cells of PBMC, plaque and synovial fluid projected on an atherosclerosis CD4$^+$ T-cells reference UMAP (rUMAP). **b.** Atherosclerosis and psoriatic arthritis CD8$^+$ T-cells of PBMC, plaque and synovial fluid projected on an atherosclerosis CD8$^+$ T-cells reference UMAP (rUMAP). **c.** rUMAP projecting clonal expansion levels of CD4$^+$ T-cells in atherosclerosis and psoriatic arthritis. **d.** Quantification of clonal expansion levels of CD4$^+$ T-cells in atherosclerosis, split over PBMC and tissue. **e.** rUMAP projecting clonal expansion levels of CD8$^+$ T-cells in atherosclerosis and psoriatic arthritis. **f.** Barplot displaying quantification of clonal expansion levels of CD8$^+$ T-cells in atherosclerosis, split over PBMC and tissue. **g.** rUMAP projecting tissue enrichment scores of clonotypes in CD4$^+$ T-cells of atherosclerosis and psoriatic arthritis. **h.** Barplot with quantification of tissue enrichment scores of CD4$^+$ T-cells in atherosclerosis and psoriatic arthritis, split by PBMC, and tissue. **i.** rUMAP projecting tissue enrichment scores of clonotypes in CD8$^+$ T-cells of atherosclerosis and psoriatic arthritis.. **j.** Quantification of tissue enrichment scores of CD8$^+$ T-cells in atherosclerosis and psoriatic arthritis, split by PBMC, and tissue. **k-n.** Dotplots with average expression of genes characterizing the genes underlying the overlap between atherosclerosis and psoriatic arthritis in CD4$^+$ T_{regs} (C5, **k**) and T_{effs} (C3, **l**) and in CD8$^+$ T_{effs} (C3, **m**; C5**;** **n**). Clonotype expansion levels: Single (1 occurrence), Medium (>0.1 & ≤1%), Large (>1 & ≤10%), Hyperexpanded (>10%), percentage of respectively CD4$^+$ and CD8$^+$ T-cells. Tissue enrichment scores: Tissue-enriched (Frequency expanded clone higher in Tissue vs. PBMC), Single (1 occurrence), Unenriched (Frequency expanded clone similar in PBMC vs. Tissue), PBMC-enriched (Frequency expanded clone higher in PBMC vs Tissue).

Discussion

Atherosclerosis has a long history of being treated as metabolic and/or lifestyle disease, with its inflammatory component being overlooked as a potential target of intervention. Ground-breaking work earlier this century has shown that inflammation is an integral part of the disease pathophysiology and significant health benefits can be obtained by intervening in inflammatory cascades. Our work here takes these observations a step further and suggests that atherosclerosis is an autoimmune-like disease, with autoreactive T-cells driving the inflammation process inside the plaque (**Fig. 7**). Classic autoimmune diseases that involve inflammation of distinct tissue, such as Type I diabetes, multiple sclerosis, and rheumatoid and psoriatic arthritis are usually associated with specific HLA Class II alleles, suggesting a pathogenic CD4$^+$ T-cell response is a major cause of disease. Moreover, accumulation of antigen-specific T-cells at the site of inflammation is a hallmark of autoimmune disease. The absence of clear associations of HLA alleles and atherosclerosis argue against the autoimmune theory in CVD[32], yet the multifactorial nature of the disease and the large population that it affects, make such associations difficult to establish. Accumulation of T-cells in atherosclerotic plaques however is well established. Moreover, earlier studies investigating TCR diversity using TCRβ sequencing in the plaque indicated an increased clonality in the lesions compared to blood samples from CVD patients.[33] By taking advantage of scTCRseq here, we can combine data on distribution of TCRs with their activation state and functionality. Using this approach we show that a select number of effector CD4⁺ T-cells and CD8⁺ T-cells accumulate in the lesions and likely undergo antigen-specific activation similar to autoimmune diseases such as psoriatic arthritis. Recent work by Chowdhury *et al*. using a similar approach reached the same conclusion[10], however by using matched PBMC controls we were able to determine that a large fraction of clonally expanded CD8⁺ T-cells did not specifically accumulate in the plaque and were equally represented or even overrepresented in the circulation. One CD8⁺ T-cell clone in particular, whose Vα TCR sequence was identified as specific for CMV, was hyperexpanded and accounted for a significant percentage of clonally expanded T-cells in the plaque, while also contributing to the clonally expanded CD8⁺ T-cell pool in the PBMC of this patient. Moreover, this clone did not show a signature of recent antigen encounter. Apart from classical CD4⁺ and CD8⁺ T-cells, we also identified a proinflammatory MAIT population. MAITs have been described in multiple autoimmune and inflammatory diseases, including psoriatic arthritis, with contradicting or unknown contributions to disease development. How MAITs contribute to atherosclerosis development and whether they are activated through their non-polymorphic MHC class I-like protein MR1 or through TCR independent activation induced by i.e. IL-12 and IL-18[34-36], needs further elucidation.

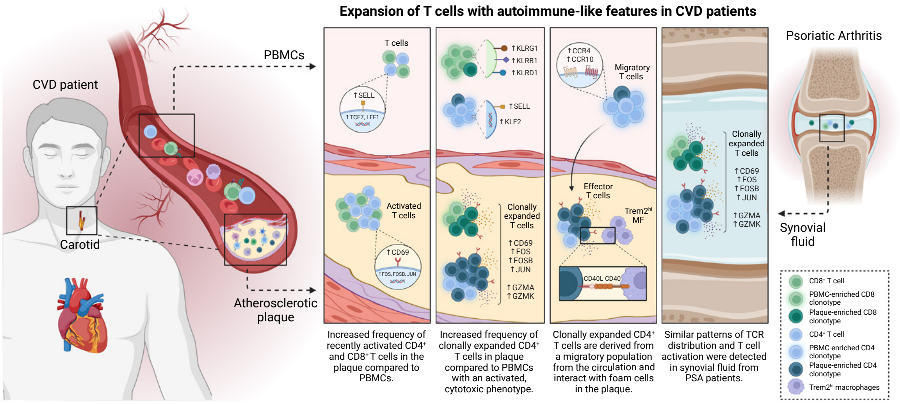

Increased frequency of recently activated CD4⁺ and CD8⁺ T cells in the plaque compared to PBMCs.

Increased frequency of clonally expanded CD4⁺ T cells in plaque compared to PBMCs with an activated, cytotoxic phenotype.

Clonally expanded CD4⁺ T cells are derived from a migratory population from the circulation and interact with foam cells in the plaque.

Similar patterns of TCR distribution and T cell activation were detected in synovial fluid from PSA patients.

Fig. 7. Schematic presentation of the main conclusions.

By instead focusing on the clonally enriched T-cells specific for the plaque, we observed that one subset of effector CD4⁺ T-cells was significantly enriched in clonally expanded TCRs and expressed genes indicative of recent antigen engagement. Although we found two such populations in the CD8⁺ T-cells, their clonal enrichment was less pronounced. Interestingly, we also observed an antigen activation signature in the plaque residing T_{regs} suggesting these T-cells undergo antigen-specific interactions in the plaque. However these T_{regs} did not show significant clonal expansion, suggesting these cells do not expand in the plaque. Instead, RNA velocity analysis suggests T_{regs} are not derived from any other T-cell population we detected in PBMC or plaque. Also, we observed minimal overlapping TCR sequences between T_{reg} and other T-cells in the plaque, in contrast to the effector $CD4^+$ T-cell population, which showed significant TCR overlap with a migratory $CD4^+$ T-cell subset in the circulation. Previous work suggests that T_{regs} can lose their suppressive capacity and gain expression of proinflammatory markers.[37] A shift of autoreactive (ApoB100-specific) T_{regs} towards a T_{h17} phenotype has been associated with severity of CVD. Although the authors show in mice that this shift happens independent of the TCR clonotypes, our data argues against such a shift and suggests T_{regs} and effector $CD4^+$ T-cells do not derive from the same ancestor, but rather develop independent of one another. Alternatively, the number of TCRs detected here may not have been sufficient to find overlapping sequences between T_{regs} and effector $CD4^+$ T-cells. Also, it is unknown whether ApoB100-specific T-cells undergo antigen-specific interaction in the plaque and because the antigen-specificity of T-cells investigated in this study are unknown, it is possible we did not examine ApoB100-specific $CD4^+$ and $CD8^+$ T-cells here.

We attempted to cluster the TCRs in silico using GLIPH2 and GIANA algorithms[38,39], which are based on CDR3β similarity, as this is proposed to be an attractive way to cluster TCRs for a specific antigen together. However, a convincing clustering of plaque-enriched clonotypes was not observed in our dataset. The current clustering algorithms may have some limitations, which in our data was illustrated by co-clustering of $CD4^+$ T cell and $CD8^+$ T cell derived clonotypes, which was only resolved if the CDR3α sequence was included. Moreover, we observed diffuse clustering of clonotypes previously reported as ApoB100-specific[40] suggesting that the current algorithms are not specific enough to resolve TCR clustering in atherosclerosis. Therefore, we believe that a more stringent approach that includes both CDR3α and CDR3β needs to be developed.

As we observe antigen-specific activation in both the effector as well as T_{reg} subsets, it is currently unclear what the overall effect of TCR engagement in the lesion is. Previous work in mice has shown mixed results with $MHCII^{-/-}$ $apoE^{-/-}$ mice suggesting this interaction is protective, whereas various papers suggest a pathogenic role for $CD4^+$ T-cells in atherosclerosis.[41,42] Interestingly, our work identifies several pathways involved in costimulation and immunological synapse formation that potentially drive pathogenic interactions of effector $CD4^+$ T-cells with the M-TREM2 (foam cell) population. When limited to effector $CD4^+$ T-cell populations these may be specific and druggable targets.

For instance, the expression of *CD40LG* on the clonally enriched effector population, suggests active signaling to foam cells through CD40. This costimulatory pathway and that of other TNF superfamily member has been extensively studied in mouse models of atherosclerosis and is subject of a clinical study.[43,44] The observation of antigen-specific T_{reg} interaction also provides a rationale for potential therapeutic possibilities, such as expanding these cells by means of vaccination or development of tolerogenic CAR T-cells. Identification of the antigen(s) driving T_{reg} interaction in the plaque will be crucial for this development. Potential antigens such ApoB100, Heat Shock Proteins, and fibronectin have been suggested as potential self-antigens and have shown therapeutic potential as antigens in mouse models[45–47] and may serve as potential starting point for vaccine development. Thus, here we highlight an autoimmune component to the pathophysiology of atherosclerosis, and confirm a rationale for immunotherapeutic interventions in cardiovascular disease.

Methods

Patient cohorts

For flow cytometry (Cohort 1) and bulk TCRβ sequencing (Cohort 3), whole blood and atherosclerotic plaques were obtained from respectively 61 and 10 patients that underwent carotid endarterectomy surgery (CEA) at the Haaglanden Medical Center Westeinde (HMC; The Hague, The Netherlands). The study was approved by the Medical Ethics Committee of the HMC (Study approval number Cohort 1: 17-046, protocol number NL57482.098.17 and Cohort 3: Z19.075, protocol number NL71516.058.19). For single-cell TCR sequencing, whole blood and atherosclerotic plaques were obtained from 3 male patients that underwent CEA (Cohort 2). Patients were included in the AtheroExpress biobank (AE, www.atheroexpress.nl), an ongoing biobank study at the University Medical Centre Utrecht (UMCU).[48] The study was approved by the Medical Ethics Committee of the UMCU (Study approval number: TME/C-01.18, protocol number 03/114). All blood samples were collected by venipuncture prior to surgery. Atherosclerosis specimens were obtained from primary CEAs, restenotic plaques were excluded due to their different plaque composition as compared to primary atherosclerotic plaques.[49] Informed consent was obtained from all patients involved in this study.

Whole blood processing

Peripheral venous blood was collected in K2-EDTA blood tubes (BD Vacutainer). For single-cell TCR sequencing, blood was processed within 10 minutes after withdrawal (Cohort 2). For both Cohort 1 and 2, blood was diluted 1:2 in Phosphate Buffered Saline (PBS) containing 2% Fetal Calf Serum (FCS). A density gradient was created using SepMate™

PBMC isolation tubes (STEMCELL Technologies) containing Ficoll-Paque Premium™ (GE Healthcare). Cells were centrifuged at 1200xg for 10 minutes at room temperature. The intermediate layer containing peripheral blood mononuclear cells (PBMC) was isolated and washed twice with PBS + 2% FCS (250xg, 10 minutes, room temperature). Cells were taken up in PBS + 1% Bovine Serum Albumin (BSA) until further processing. For Cohort 3, whole blood samples were lysed twice with ACK lysis buffer in PBS(1:10) for 10 minutes at RT and washed with PBS (300xg, 5 minutes). Cells were taken up in RPMI + 1% FCS and cryostored in Cryostor cell cryopreservation medium (Sigma-Aldrich) until further use.

Human atherosclerotic plaque cell isolation

Human carotid plaques were collected during CEA; the culprit segment (5 mm) was used for histology and embedded in paraffin as described elsewhere.[48] In brief, culprit segments were fixed in 4% formaldehyde and decalcified in 10% EDTA pH 7.5. Afterwards, culprit segments were embedded in paraffin. Time between surgical removal and plaque processing did not exceed 10 minutes. The inclusion of a small medial layer in the dissected tissue could not be excluded during the surgical procedure. The remainder of the plaque washed in RPMI and minced into small pieces with a razor blade. The tissue was then digested in RPMI 1640 containing 2.5 mg/mL Collagenase IV (ThermoFisher Scientific), 0.25 mg/mL DNAse I (Sigma), 2.5 mg/mL Human Albumin Fraction V (MP Biomedicals) at 37°C for 30 minutes. In Cohort 2, 1 µM Flavopiridol (Selleckchem) was added to the digestion mixture. Subsequently, the plaque cell suspension was filtered through a 70 µm cell strainer and washed with RPMI 1640. Cells were kept in RPMI 1640 with 1% Fetal Calf Serum until subsequent staining for flow cytometry (Cohort 1), Feature Barcoding and fluorescence-activated cell sorting (Cohort 2) or cryostored in Cryostor cell cryopreservation medium (Sigma-Aldrich) until further use.

Flow cytometry

Single cell suspensions from blood and plaque from Cohort 1 were stained with a mixture of extracellular antibodies for 30 minutes at 37°C (**Supplementary Table 4**). All measurements were performed on a Cytoflex S (Beckman and Coulter, USA) and analysed with FlowJo v10.7 (Treestar, San Carlos, CA, USA). A Shapiro log normality test was performed and a two-tailed Mann Whitney test was performed using GraphPad analysis software to determine significance.

Antibody staining for Feature Barcoding and fluorescent activated cell sorting

PBMC

PBMCs of Cohort 2 were stained with TotalSeq-C antibodies against CD3, CD4, CD8 and CD14 (**Supplemental Table 4**). Antibody pools containing 0.25 µg per antibody were prepared in labeling buffer (PBS + 1% BSA), spun down at 14.000xg for 10 minutes at room temperature and supernatant was collected for further staining. First, cells were stained with Human Trustain FcX (Biolegend) for 10 minutes at 4°C. Next, the antibody pool supernatant was added and incubated for 30 minutes at 4°C. Cells were washed thrice with labeling buffer at 400xg for 5 minutes at 4°C. Next, cells were taken up in PBS + 0.4% BSA and further processed with 10X genomics.

Plaque

Single cell suspensions of plaques of Cohort 2 were stained with TotalSeq-C antibodies against CD3, CD4, CD8 and CD14 (**Supplemental Table 4**). Antibody pools containing 0.25 µg/antibody and plaque (1 µg/antibody) single cell suspensions were prepared in labeling buffer (PBS + 1% BSA), spun down at 14.000xg for 10 minutes at room temperature and supernatant was collected for further staining. First, cells were stained with Human Trustain FcX (Biolegend) for 10 minutes at 4°C. Next, the antibody pool supernatant was added together with Calcein AM (1:1000; ThermoFisher), Hoechst (1:000; ThermoFisher) and CD45-PECy7 (1:200, Clone HI30, BD Biosciences) and incubated for 30 minutes at 4°C. Cells were washed thrice with labeling buffer at 400xg for 5 minutes at 4°C. Next, cells were taken up in PBS + 2% FBS. Live CD45$^+$ plaque cells were sorted using the BD FACS Aria II (BD Biosciences) in PBS + 0.04% BSA and further processed with 10X genomics.

Single-cell TCR sequencing by 10X Genomics

Single-cell TCR sequencing was performed on PBMCs and live CD45$^+$ plaque cell suspensions from Cohort 2 using the 10X Genomics 5′ Single Cell Immune Profiling technology (10X Genomics, USA). Sequencing libraries were prepared using the 5′ V1.1 chemistry following standard 10X Genomics protocol (10X Genomics, USA). Sequencing was performed using the Illumina Novaseq 6000 (Novogene).

Bulk TCRβ sequencing

Genomic DNA was extracted from plaque single cell suspensions and matched PBMC samples (Cohort 3) using a DNA extraction kit in accordance to the manufacturer's instructions (Qiagen, Hilden Germany). Sequencing of the VDJ locus was performed using the Adaptive Biotechnologies (Seattle WA) TCRβ sequencing platform.

Single-cell TCR sequencing data processing , clustering, and clonotype quantification

Single-cell TCR sequencing data analyses were executed in R-4.0.1 and R-4.1.3 environments, primarily using Seurat (version 4.0.0 – 4.1.1).[50,51] scTCR-seq data were processed as previously described.[51,52] In short, reads were filtered for mitochondrial, ribosomal genes, and long noncoding RNA genes. To remove apoptotic cells, low quality cells, and doublets, only cells with a gene expression below 2% for KCNQ1OT1, below 2% for UGDH-AS1 , below 2 % for GHET1, and expressing between 200 and 5000 genes were used for further analysis. QC-filtered PBMC and plaque Seurat-objects were first merged per patient, after which the patient-merged Seurat-objects were normalized using the SCT method, integrated using rpca reduction with, and clustered according to the Seurat "scRNA-seq integration"-vignette. VDJ-sequencing data were imported into Seurat using the combineExpression function of scRepertoire (version 1.4.0).[53] The complete integrated dataset was mapped to the pbmc_multimodal.h5seurat dataset (https://atlas.fredhutch.org/data/nygc/multimodal/pbmc_multimodal.h5seurat) to transfer cell type labels to the integrated Seurat-object.

For subclustering, T-cells were selected from the complete integrated dataset, taking the clusters with protein expression of CD3, CD4 and CD8, and without CD14 expression (ADT assay). Before reclustering the T-cells, variable TCR genes were removed from the variable genes list, before PCA and clustering to avoid clustering based on TCR, interfering with clustering on T-cell phenotype. Yet, TCR genes were not removed from the data set. Separate CD4$^+$ T-cell and CD8$^+$ T-cell objects were then created by subsetting the T-cell object based on respectively protein expression of CD4>0.75 and CD8>1.0 in the ADT assay. Custom clonotype counting functions were used to quantify the clonotype content of the individual samples based on the amino acid sequences of the TCRs. Clonotype frequencies relating to the total TCR repertoire per patient, per tissue are depicted in the atherosclerosis figures. Volcano plots were created using EnhancedVolcano (version 1.8.0).[54] For all Volcano plots, the FindMarkers function of Seurat was used to define differential genes between both groups by using a non-parametric Wilcoxon Rank sum test to determine significance. To assess the differentiation trajectories of the CD4$^+$ T-cells and CD8$^+$ T-cells Monocle (version 3) and velocyto.R (version 0.6) were utilized.[22,55] To assess possible interactions of antigen presenting cells and T-cells in the plaque CellChat (version 1.4.0) was utilized.[25]

Definition of clonotype expansion levels and tissue-enrichment scores

The TCR amino acid sequences were used to define the clonotypes. The clonotype abundance of a clonotype was calculated as the percentage of cells expressing a certain clonotype within a tissue of a patient, divided by the total number of cells in which a TCR was detected in the same tissue of the same patient. Based on the number and percentage of cells expressing the same Clonotype, Clonotypes were classified as either, Hyperexpanded, Large, Medium, Small, or Single in the tissues of the patients (**Supplementary Table 5**). Furthermore the tissue enrichment of clonotypes was determined according to the parameters listed in **Supplementary Table 6**.

Integration with psoriatic arthritis scTCRseq data

T-cells from our scTCRseq atherosclerosis dataset were compared with TCRseq data from donor-matched PBMC and Synovial Tissue from Psoriatic arthritis (PSA) patients (ArrayExpress: E-MTAB-9492, European Genome-phenome Archive: EGAS00001002104).[31] The same QC, and processing steps were performed for the PSA dataset as described above for our atherosclerosis data set. Subsequently, the integrated PSA dataset was mapped to the UMAP reduction of our complete T-cell object, using our atherosclerosis dataset as reference. Because CD4$^+$ T-cells and CD8$^+$ T-cells could not be separated cleanly based on the clustering and the PSA dataset does not contain protein expression data, the atherosclerosis dataset and the PSA dataset were divided based on the predicted cell type (CD4 T-cell or CD8 T-cell), derived from the pbmc_multimodal.h5seurat dataset. Subsequently, the atherosclerosis and PSA CD4$^+$ T-cell and CD8$^+$ T-cell datasets were split by patient and reintegrated as previously described for the atherosclerosis object, to form a CD4$^+$ T-cell object and a CD8$^+$ T-cell object containing atherosclerosis and PSA derived T-cells. Then, the integrated datasets were mapped to our original CD4$^+$ T-cell and CD8$^+$ T-cell UMAP reductions. Since the PSA dataset is devoid of naïve T-cells due to the T-cell isolation procedure utilized by Penkava *et al.* , naïve T-cell clusters were removed from the CD4$^+$ T-cell dataset (cluster1 and 2) and CD8$^+$ T-cell dataset (cluster 6) before quantification of the clonotype abundance.[31]

Data availability

The raw single-cell TCR sequencing data from the Athero-Express cohort are not publicly available due to research participant privacy/consent. These data and the bulk TCRβ sequencing data can be accessed via DataverseNL at this address: https://doi.org/10.34894/DDYKLL. There are restrictions on use by commercial parties, and on sharing openly based on (inter)national laws and regulations and the written informed consent. Therefore, these data (and additional clinical data) are only available upon discussion and signing a Data Sharing Agreement (see Terms of Access in DataverseNL) and within a specially designed UMC Utrecht provided environment.

Open source single-cell TCR sequencing data from donor-matched PBMC and Synovial Tissue from Psoriatic arthritis (PSA) patients that we used in this study are publicly available (ArrayExpress: E-MTAB-9492, European Genome-phenome Archive: EGAS00001002104).[31]

Code availability

In silico data analysis was performed using custom made R scripts designed specifically for this study and/or based on the recommended pipelines from pre-existed packages listed above. R scripts are available via Zenodo (https://doi.org/10.5281/zenodo.7415207).

Supplemental Tables

For supplemental tables see https://doi.org/10.1038/s44161-022-00208-4

Ackowledgements

This work was supported by The Netherlands Heart Foundation [CVON2017-20: GENIUS II supporting JK, MW, GP, MACD, IB, BS], Dekker Fellowship [2018T051 to ACF]; Spark-Holding BV [grant number 2015B002 to MW]; NWO-ZonMW [PTO program grant number 95105013, supporting MACD, IB, JK]; the European Union [ITN-grant EPIMAC to MW]; Fondation Leducq [Transatlantic Network Grants to MW and GP]; EU 755320 Taxinomisis grant [supporting GJdB, AB, GP] and European Research Area Network on Cardiovascular diseases [ERA-CVD, 2018T092 supporting MJMJ, BS and 2019T107 supporting JM, ACF]; NWO Veni [VI.Veni.212.196 to KHMP]; NWO-ZonMW [Open competition 09120011910025 to MW]. Established investigator of the Netherlands Heart Foundation [2019T067, supporting EH, LD, IB].

We would like to thank Single Cell Discoveries (Utrecht) for processing 10X genomics samples. Study set up figures and the graphical abstract were created in BioRender.

Author contributions

M.A.C.D., F.H.S., I.B, J.K, A.C.F and B.S. drafted the manuscript and designed the figures. J.A.H.M.P, L.G., A.W., H.J.S and G.J.B. performed carotid endarterectomy procedures and collected patient material. M.A.C.D., A.B., E.H., L.D., J.M., M.N.A.B.K and M.J.M.J executed the human plaque processing, FACS and flow cytometry. M.A.C.D., K.H.M.P., F.S, J.K., I.B., B.S. participated in conceptualization, data interpretation and provided critical feedback on the manuscript. J.K., M.W., G.P., I.B and B.S participated in the conceptualization, funding and supervision of the scRNAseq experiments and analysis and finalization of the manuscript. All authors provided feedback on the research, analyses and manuscript.

Competing interests

The authors declare no competing interests.

References

1. Ridker, P. M. *et al.* Antiinflammatory Therapy with Canakinumab for Atherosclerotic Disease. *N. Engl. J. Med.* **377**, 1119–1132 (2017).
2. Nidorf, S. M. *et al.* Colchicine in Patients with Chronic Coronary Disease. *N. Engl. J. Med.* **383**, 1838–1847 (2020).
3. Depuydt, M. A. C. *et al.* Microanatomy of the Human Atherosclerotic Plaque by Single-Cell Transcriptomics. *Circ. Res.* **127**, 1437–1455 (2020).
4. Fernandez, D. M. *et al.* Single-cell immune landscape of human atherosclerotic plaques. *Natuere Med.* **25**, 1576–1588 (2019).
5. Stemme, S. *et al.* T lymphocytes from human atherosclerotic plaques recognize oxidized low density lipoprotein. *Med. Sci.* **92**, 3893–3897 (1995).
6. Wolf, D. *et al.* Pathogenic Autoimmunity in Atherosclerosis Evolves From Initially Protective Apolipoprotein B 100-Reactive CD4 + T-Regulatory Cells. *Circulation* **142**, 1279–1293 (2020).
7. Roy, P. *et al.* Immunodominant MHC-II (Major Histocompatibility Complex II) Restricted Epitopes in Human Apolipoprotein B. *Circ. Res.* **131**, 258–276 (2022).
8. Benne, N. *et al.* Anionic 1,2-distearoyl-sn-glycero-3-phosphoglycerol (DSPG) liposomes induce antigen-specific regulatory T cells and prevent atherosclerosis in mice. *J. Control. Release* **291**, 135–146 (2018).
9. Gisterå, A. *et al.* Vaccination against T-cell epitopes of native ApoB100 reduces vascular inflammation and disease in a humanized mouse model of atherosclerosis. *J. Intern. Med.* **281**, 383–397 (2017).
10. Chowdhury, R. R. *et al.* Human Coronary Plaque T Cells Are Clonal and Cross-React to Virus and Self. *Circ. Res.* **130**, 1510–1530 (2022).
11. Cibrián, D. & Sánchez-Madrid, F. CD69: from activation marker to metabolic gatekeeper. *Eur. J. Immunol.* **47**, 946–953 (2017).
12. Schenkel, J. M. *et al.* T cell memory. Resident memory CD8 T cells trigger protective innate and adaptive immune responses. *Science* **346**, 98–101 (2014).
13. Kranzer, K. *et al.* CpG-oligodeoxynucleotides enhance T-cell receptor-triggered interferon-gamma production and up-regulation of CD69 via induction of antigen-presenting cell-derived interferon type I and interleukin-12. *Immunology* **99**, 170–178 (2000).
14. Mohr, A., Malhotra, R., Mayer, G., Gorochov, G. & Miyara, M. Human FOXP3+ T regulatory cell heterogeneity. *Clin. Transl. Immunol.* **7**, 1–11 (2018).
15. Wherry, E. J. & Kurachi, M. Molecular and cellular insights into T cell exhaustion. *Nat. Rev. Immunol.* **15**, 486–499 (2015).
16. Khan, O. *et al.* TOX transcriptionally and epigenetically programs CD8 + T cell exhaustion. *Nature* **571**, 211–218 (2019).
17. Padhan, K. & Varma, R. Immunological synapse: A multi-protein signalling cellular apparatus for controlling gene expression. *Immunology* **129**, 322–328 (2010).
18. Bagaev, D. V. *et al.* VDJdb in 2019: database extension, new analysis infrastructure and a T-cell receptor motif compendium. *Nucleic Acids Res.* **48**, D1057–D1062 (2020).
19. Vorkas, C. K. *et al.* Single-Cell Transcriptional Profiling Reveals Signatures of Helper, Effector, and Regulatory MAIT Cells during Homeostasis and Activation. *J. Immunol.* **208**, 1042–1056 (2022).
20. Liuzzo, G. *et al.* Monoclonal T-Cell Proliferation and Plaque Instability in Acute Coronary Syndromes. *Circulation* **102**, 2883–2888 (2000).

21. Liuzzo, G. *et al*. Unusual CD4+CD28null T Lymphocytes and Recurrence of Acute Coronary Events. *J. Am. Coll. Cardiol.* **50**, 1450–1458 (2007).
22. La Manno, G. *et al*. RNA velocity of single cells. *Nature* **560**, 494 (2018).
23. Ali, A. J., Makings, J. & Ley, K. Regulatory T Cell Stability and Plasticity in Atherosclerosis. *Cells* **9**, (2020).
24. Wang, X. *et al*. Visualizing CD4 T-cell migration into inflamed skin and its inhibition by CCR4/CCR10 blockades using in vivo imaging model. *Br. J. Dermatol.* **162**, 487–496 (2010).
25. Jin, S. *et al*. Inference and analysis of cell-cell communication using CellChat. *Nat. Commun.* **12**, (2021).
26. Foks, A. C. & Kuiper, J. Immune checkpoint proteins: exploring their therapeutic potential to regulate atherosclerosis. *Br. J. Pharmacol.* **174**, 3940–3955 (2017).
27. Kwon, I. O. *et al*. CD99 activates T cells via a costimulatory function that promotes raft association of TCR complex and tyrosine phosphorylation of TCR ζ. *Exp. Mol. Med.* **39**, 176–184 (2007).
28. Bixel, G. *et al*. Mouse CD99 participates in T-cell recruitment into inflamed skin. *Blood* **104**, 3205–3213 (2004).
29. Calandra, T. & Roger, T. Macrophage migration inhibitory factor: a regulator of innate immunity. *Nat. Rev. Immunol.* **3**, 791–800 (2003).
30. D'Acquisto, F. *et al*. Annexin-1 modulates T-cell activation and differentiation. *Blood* **109**, 1095–1102 (2007).
31. Penkava, F. *et al*. Single-cell sequencing reveals clonal expansions of pro-inflammatory synovial CD8 T cells expressing tissue-homing receptors in psoriatic arthritis. *Nat. Commun.* **11**, (2020).
32. Björkbacka, H. *et al*. Weak associations between human leucocyte antigen genotype and acute myocardial infarction. *J. Intern. Med.* **268**, 50–58 (2010).
33. Lin, Z. *et al*. Deep sequencing of the T cell receptor β repertoire reveals signature patterns and clonal drift in atherosclerotic plaques and patients. *Oncotarget* **8**, 99312–99322 (2017).
34. Treiner, E. *et al*. Selection of evolutionarily conserved mucosal-associated invariant T cells by MR1. *Nature* **422**, 164–169 (2003).
35. Godfrey, D. I., Koay, H. F., McCluskey, J. & Gherardin, N. A. The biology and functional importance of MAIT cells. *Nat. Immunol.* **20**, 1110–1128 (2019).
36. Van Wilgenburg, B. *et al*. MAIT cells are activated during human viral infections. *Nat. Commun.* **7**, (2016).
37. Kleinewietfeld, M. & Hafler, D. A. The plasticity of human Treg and Th17 cells and its role in autoimmunity. *Semin. Immunol.* **25**, 305–312 (2013).
38. Huang, H., Wang, C., Rubelt, F., Scriba, T. J. & Davis, M. M. Analyzing the Mycobacterium tuberculosis immune response by T-cell receptor clustering with GLIPH2 and genome-wide antigen screening. *Nat. Biotechnol. 2020 3810* **38**, 1194–1202 (2020).
39. Zhang, H., Zhan, X. & Li, B. GIANA allows computationally-efficient TCR clustering and multi-disease repertoire classification by isometric transformation. *Nat. Commun. 2021 121* **12**, 1–11 (2021).
40. Saigusa, R. *et al*. Single cell transcriptomics and TCR reconstruction reveal CD4 T cell response to MHC-II-restricted APOB epitope in human cardiovascular disease. *Nat. Cardiovasc. Res. 2022 15* **1**, 462–475 (2022).
41. Wigren, M. *et al*. Lack of Ability to Present Antigens on Major Histocompatibility Complex Class II Molecules Aggravates Atherosclerosis in ApoE -/- Mice. *Circulation* **139**, 2554–2566 (2019).
42. Tabas, I. & Lichtman, A. H. Monocyte-Macrophages and T Cells in Atherosclerosis. *Immunity* **47**, 621–634 (2017).

43. Smeets, E., Meiler, S. & Lutgens, E. Lymphocytic tumor necrosis factor receptor superfamily co-stimulatory molecules in the pathogenesis of atherosclerosis. *Curr. Opin. Lipidol.* **24**, 518–524 (2013).
44. Seijkens, T. T. P. *et al*. Targeting CD40-Induced TRAF6 Signaling in Macrophages Reduces Atherosclerosis. *J. Am. Coll. Cardiol.* **71**, 527–542 (2018).
45. Chyu, K. Y. *et al*. Immunization using ApoB-100 peptide-linked nanoparticles reduces atherosclerosis. *JCI insight* **7**, (2022).
46. Van Puijvelde, G. H. M. *et al*. Induction of oral tolerance to HSP60 or an HSP60-peptide activates T cell regulation and reduces atherosclerosis. *Arterioscler. Thromb. Vasc. Biol.* **27**, 2677–2683 (2007).
47. Dunér, P. *et al*. Immunization of apoE-/- mice with aldehyde-modified fibronectin inhibits the development of atherosclerosis. *Cardiovasc. Res.* **91**, 528–536 (2011).
48. Verhoeven, B. A. N. *et al*. Athero-express: Differential atherosclerotic plaque expression of mRNA and protein in relation to cardiovascular events and patient characteristics. Rationale and design. *Eur. J. Epidemiol.* **19**, 1127–1133 (2004).
49. Hellings, W. E. *et al*. Histological characterization of restenotic carotid plaques in relation to recurrence interval and clinical presentation: a cohort study. *Stroke* **39**, 1029–32 (2008).
50. R Core Team. R: A language and environment for statistical computing. https://www.r-project.org/ (2019).
51. Butler, A., Hoffman, P., Smibert, P., Papalexi, E. & Satija, R. Integrating single-cell transcriptomic data across different conditions , technologies , and species. *Nat. Biotechnol.* **36**, 411–420 (2018).
52. Stuart, T. *et al*. Comprehensive Integration of Single-Cell Data. *Cell* **177**, 1888-1902.e21 (2019).
53. Borcherding, N., Bormann, N. L. & Kraus, G. scRepertoire: An R-based toolkit for single-cell immune receptor analysis. *F1000Research* **9**, (2020).
54. Blighe, K., Rana, S. & Lewis, M. EnhancedVolcano: Publication-ready volcano plots with enhanced colouring and labeling. (2018).
55. Cao, J. *et al*. The single-cell transcriptional landscape of mammalian organogenesis. *Nature* **566**, 496–502 (2019).

Extended Data

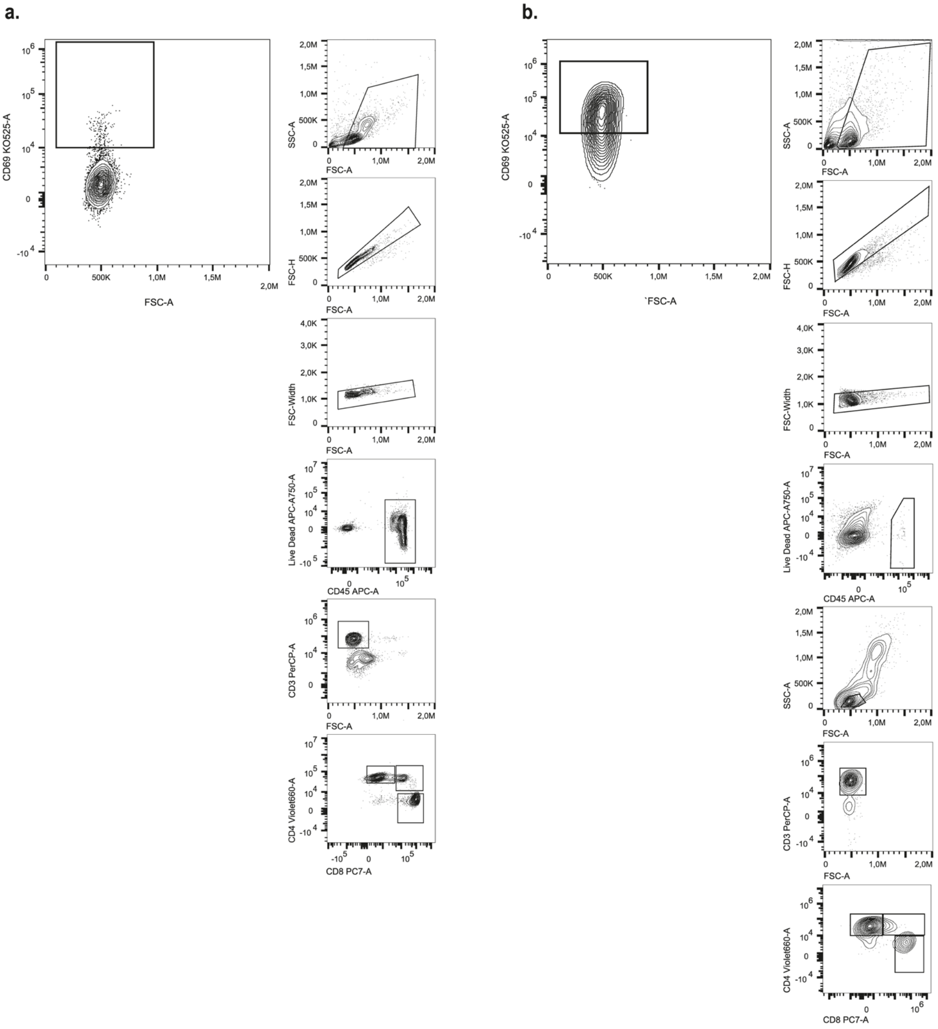

Extended Data Fig. 1. Gating strategy of flow cytometry of CD69⁺ T-cells. a. Example of gating and gating ancestry of CD69⁺ T-cells in PBMC. **b.** Example of gating and gating ancestry of CD69⁺ in the plaque.

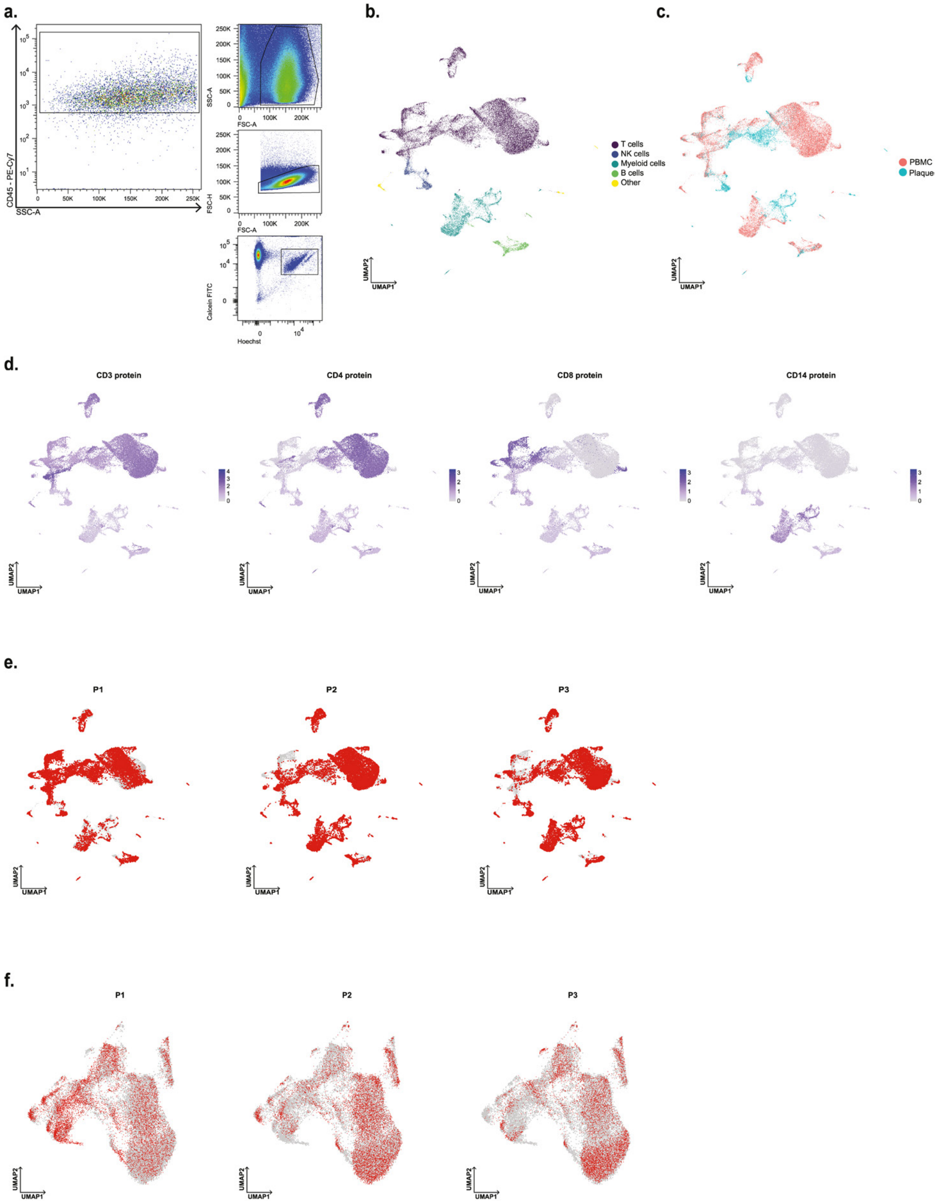

Extended Data Fig. 2. Single-cell RNA sequencing of PBMC and live CD45$^+$ plaque cells. a. Gating strategy used for fluorescent-activated cell sorting (FACS) to isolate plaque live CD45$^+$ cells for 10X Genomics and sequencing. **b.** UMAP projection of all PBMC and plaque cells, depicting multiple leukocyte types (n = 33249). **c.** UMAP visualization of tissue distribution of PBMC and plaque cells. **d.** UMAP projection of protein expression of CD3, CD4, CD8 and CD14 on all PBMC and plaque cells. **e.** Patient contribution to UMAP of all PBMC and plaque cells. Red dots indicate cells that are retrieved from the abovementioned patient. **f.** Patient contribution to UMAP of PBMC and plaque T-cells. Red dots indicate cells that are retrieved from the abovementioned patient.

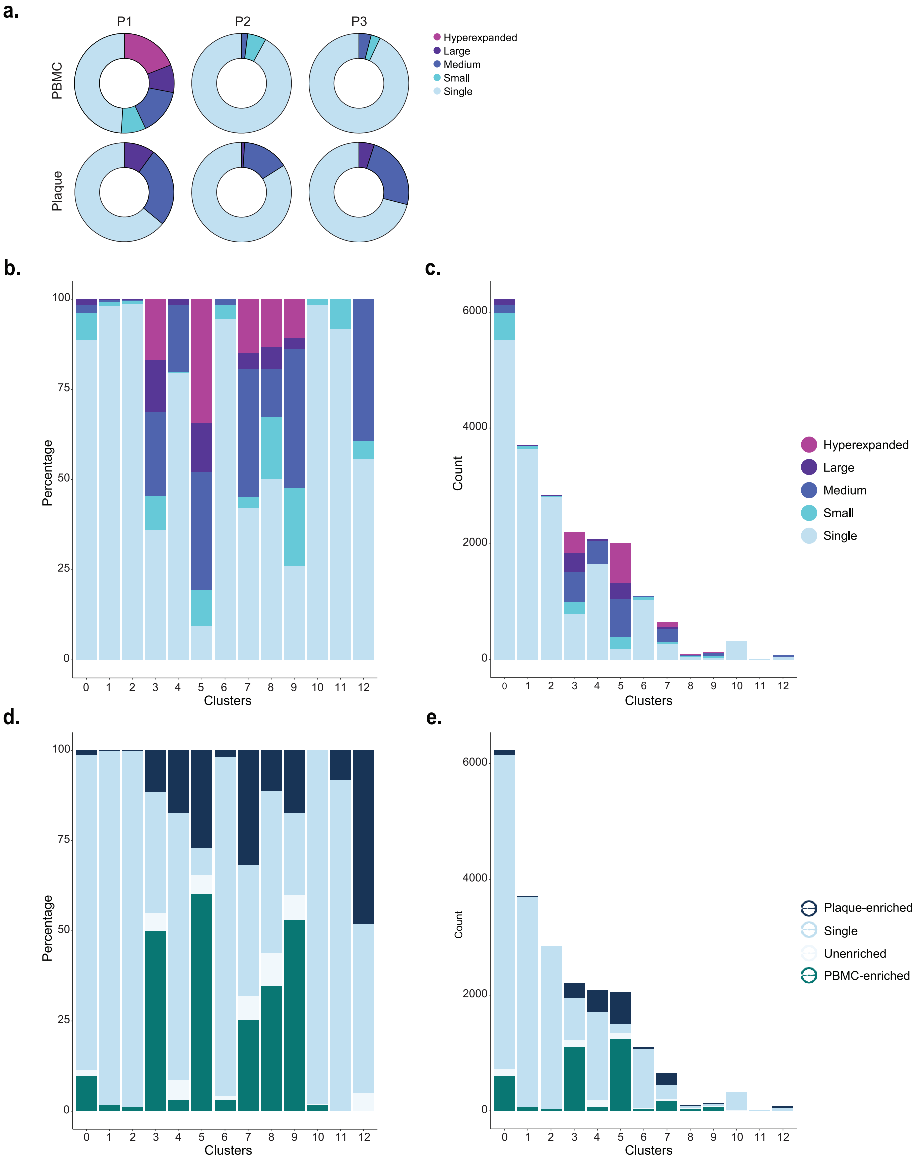

Extended Data Fig. 3. Distribution of clonal expansion levels and tissue-enrichment scores in T-cell clusters. a. Circle plots depicting clonal expansion levels of all T-cells per tissue and per patient. **b**. Barplot with relative quantification of clonal expansion levels per cluster. **c**. Barplot with absolute quantification of clonal expansion levels per cluster. **d.** Relative quantification of tissue enrichment scores per cluster. **e.** Barplot with absolute quantification of tissue enrichment scores per cluster. Clonotype expansion levels: Single (1 occurrence), Medium (>0.1 & ≤1%), Large (>1 & ≤10%), Hyperexpanded (>10%), percentage of all T-cells. Tissue enrichment scores: Plaque-enriched (Frequency expanded clone higher in Plaque vs. PBMC), Single (1 occurrence), Unenriched (Frequency expanded clone similar in PBMC vs. Plaque), PBMC-enriched (Frequency expanded clone higher in PBMC vs Plaque).

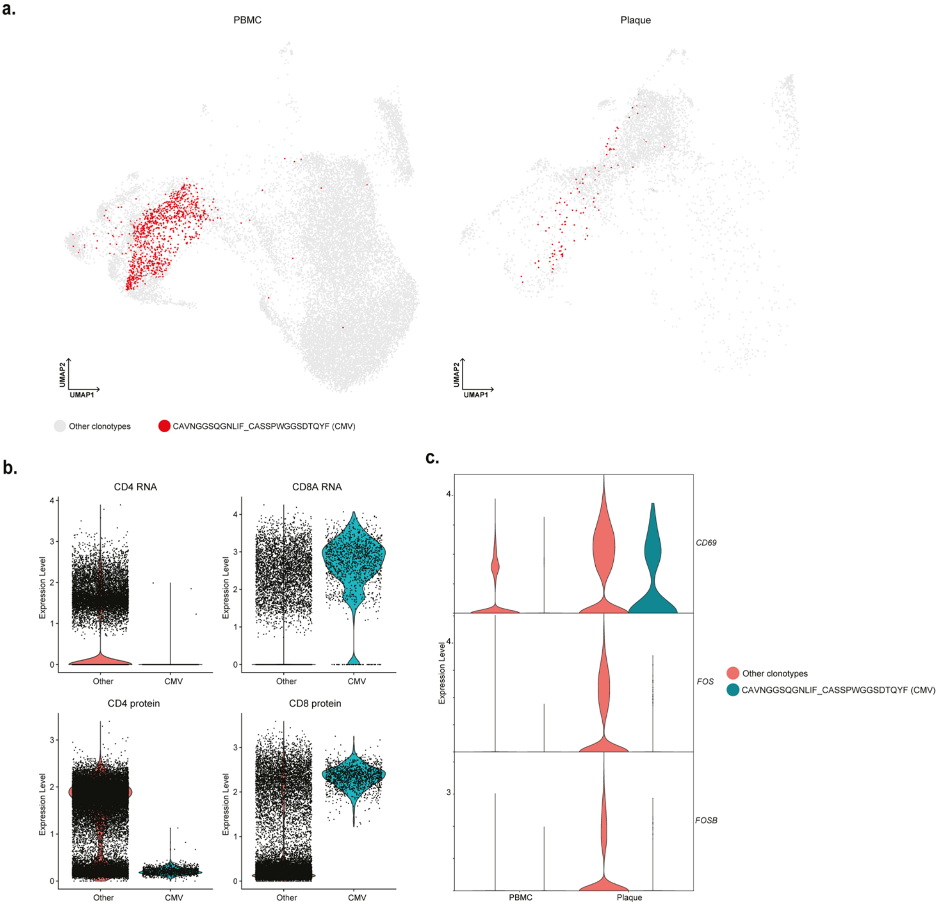

Extended Data Fig. 4. Hyperexpanded CMV clonotype does not show signs of recent T-cell activation. a. UMAP projection of clonotype CAVNGGSQGNLIF_CASSPWGGSDTQYF (CMV) on PBMC and plaque T-cells. Red dots indicate T-cells with clonotype CAVNGGSQGNLIF_CASSPWGGSDTQYF, grey dots indicate T-cells with other clonotypes. **b.** Violin plots projecting gene expression of *CD4*, *CD8A* and protein expression of CD4 and CD8 split by T-cells with and without clonotype CAVNGGSQGNLIF_CASSPWGGSDTQYF. **c.** Violin plots projecting expression of *CD69*, *FOS* and *FOSB* split by tissue and presence of clonotype CAVNGGSQGNLIF_CASSPWGGSDTQYF.

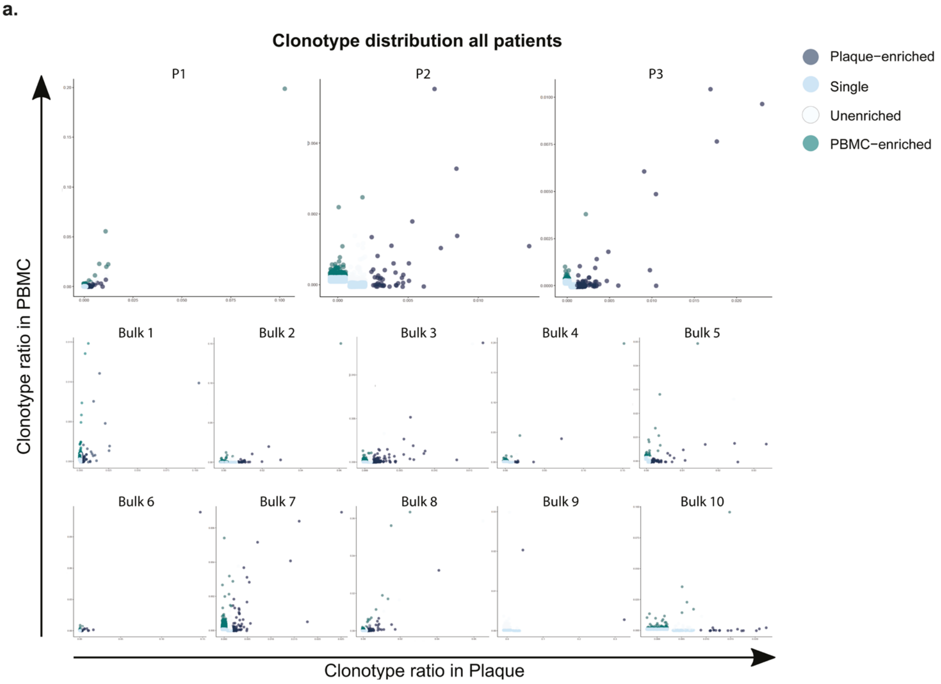

Extended Data Fig. 5. Distribution of expanded TCRs in scTCR-seq and TCR*β* bulk data sets. **a.** Scatterplot projecting frequencies of clonotypes and their tissue enrichment scores in PBMC and plaque per patient of the single-cell TCR sequencing dataset (Cohort 2) and the TCRβ bulk sequencing data set (Cohort 3). Tissue enrichment scores: Plaque-enriched (Frequency expanded clone higher in Plaque vs. PBMC), Single (1 occurrence), Unenriched (Frequency expanded clone similar in PBMC vs. Plaque), PBMC-enriched (Frequency expanded clone higher in PBMC vs Plaque).

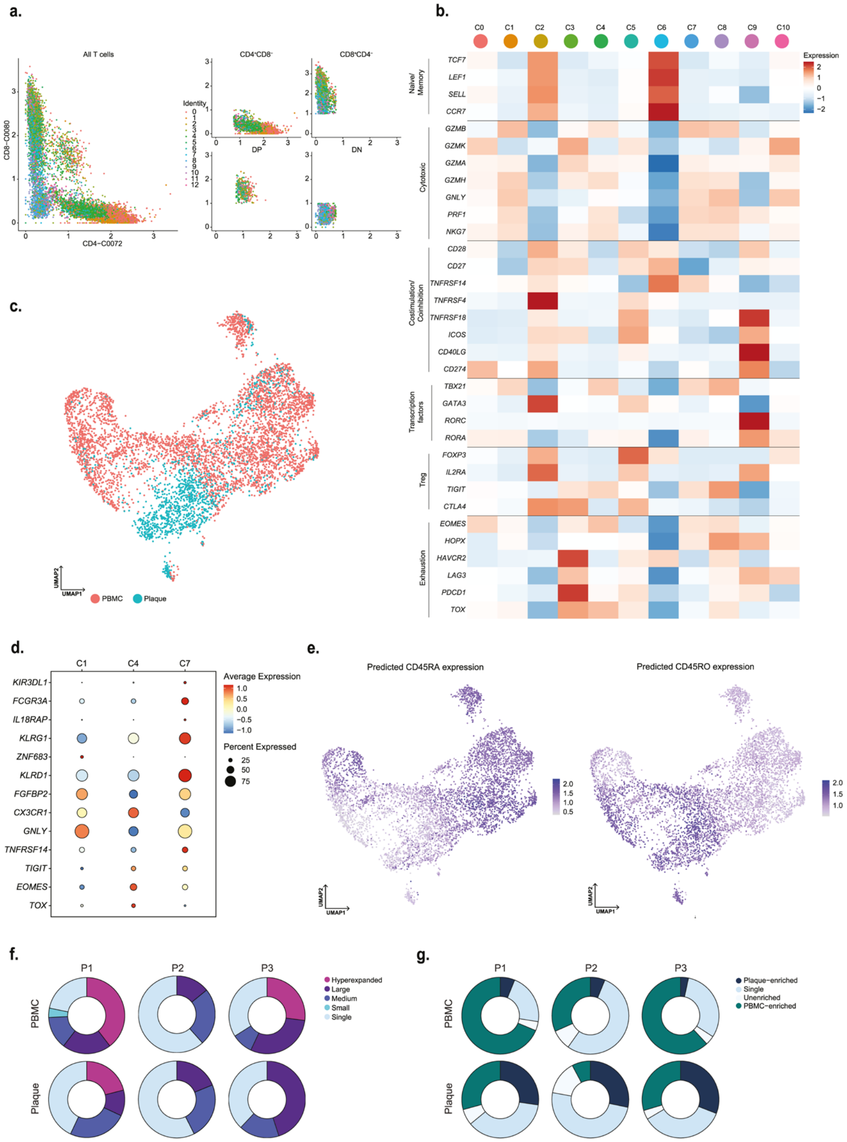

Extended Data Fig. 6. CD8$^+$ T-cell marker genes and tissue distribution. a. CD4 and CD8 protein expression on all T-cells colored by cluster ID. Visualization of selection of CD4$^+$CD8$^-$, CD4$^-$CD8$^+$, double positive (DP) and double negative (DN) cells. CD4$^+$CD8$^-$ cells were used for subclustering of CD4$^+$ T-cells. CD4$^-$CD8$^+$ cells were used for subclustering of CD8$^+$ T-cells. **b.** UMAP projection of tissue distribution of PBMC and plaque CD8$^+$ T-cells. **c.** Heatmap with expression of T-cell function-associated genes in CD8$^+$ T-cell clusters. d. Dot plot visualization of a selection of differentially regulated genes, excluding TCR complex genes, between clusters 1, 4 and 7. **e.** Predicted expression of CD45RA and CD45RO based on mapping the data with Seurat multimodal reference mapping. **f.** Circle plots depicting clonal expansion levels of CD8$^+$ T-cells per tissue and per patient. **g.** Circle plots depicting tissue-enrichment scores of CD8$^+$ T-cells per tissue and per patient.

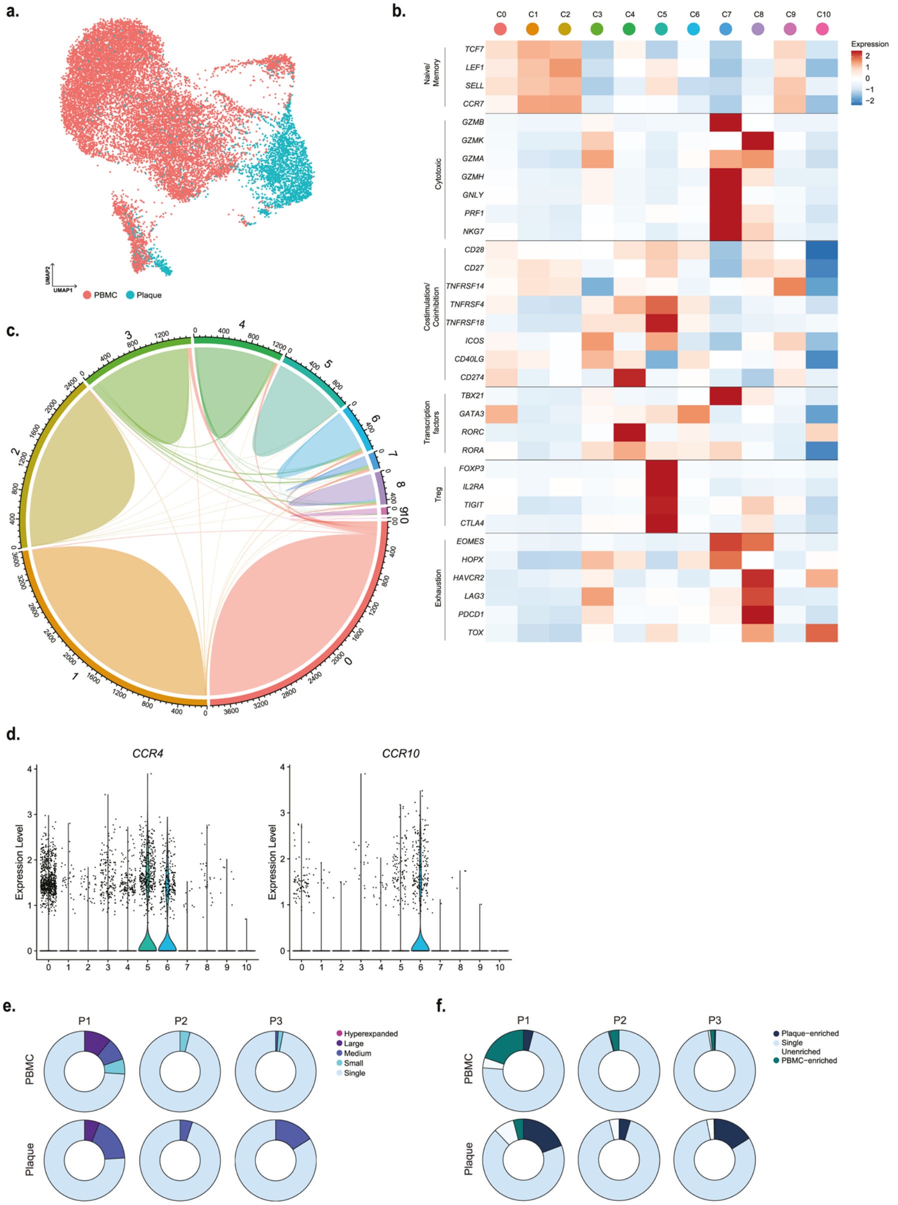

Extended Data Fig. 7. CD4$^+$ T-cell marker genes and tissue distribution. a. UMAP visualization of tissue distribution of PBMC and plaque CD4$^+$ T-cells. **b.** Heatmap with expression of T-cell function-associated genes in CD4$^+$ T-cell clusters. **c.** Circle plot visualizing the overlap of clonotypes between all CD4$^+$ clusters. Each color represents a different cluster. Axis indicates the number of TCRs. Line thickness indicates the number of overlapping clonotypes. **d.** Violin plots depicting expression of *CCR4* and *CCR10* in CD4$^+$ T-cell clusters. **e.** Circle plots depicting clonal expansion levels of CD4$^+$ T-cells per tissue and per patient. **f.** Circle plots depicting tissue-enrichment scores of CD4$^+$ T-cells per tissue and per patient.

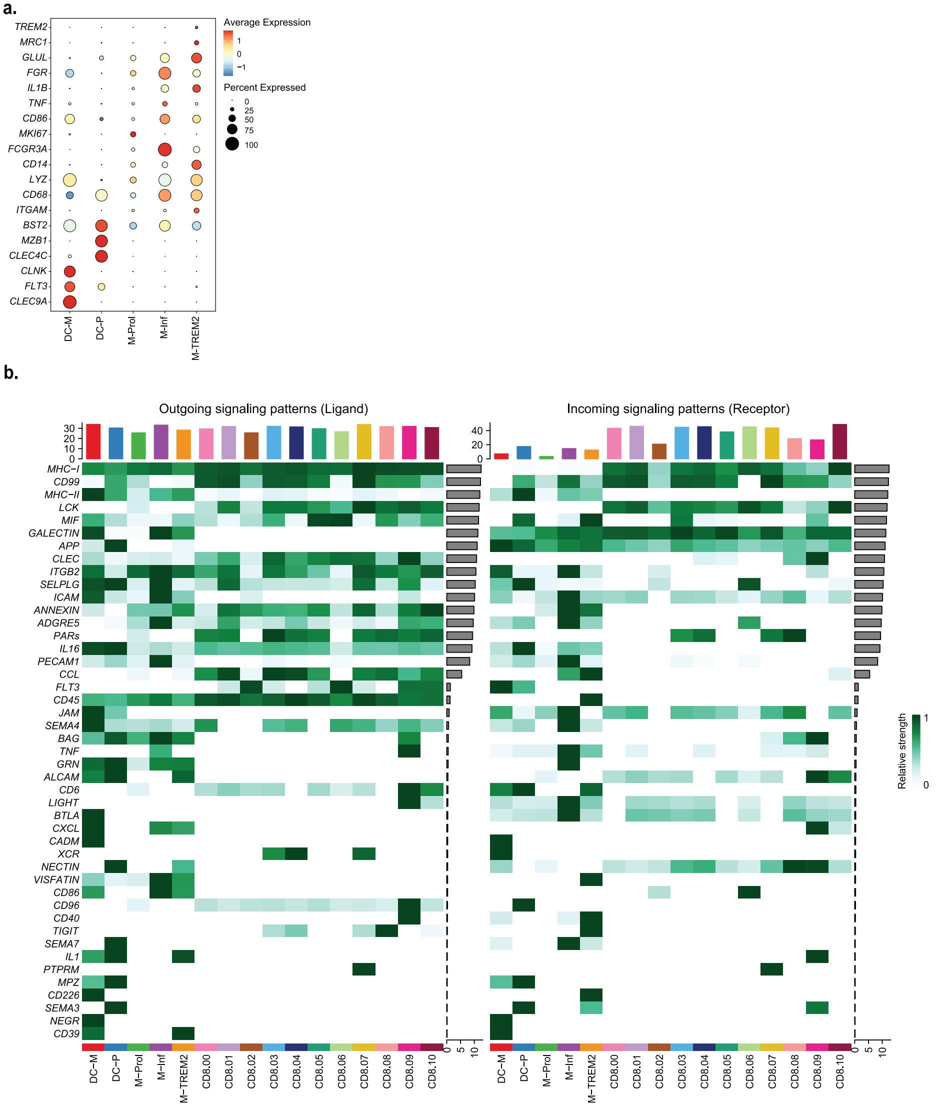

Extended Data Fig. 8. CellChat interaction pathways between CD8⁺ T-cells and myeloid cells. a. Dotplot displaying average expression of genes describing the different dendritic cell and macrophage clusters. DC-M indicates myeloid-derived dendritic cell (DC); DC-P indicates plasmacytoid DC; M-PROL indicates proliferating macrophages; M-Inf indicates inflammatory macrophage; M-TREM2 indicates TREM2^{hi} macrophages. **b.** Heatmaps displaying outgoing (Ligand) and incoming (Receptor) signaling patterns of pathways describing potential ligand-receptor interactions. Scale above heatmap indicates the relative signaling strength of a cell cluster based on all signaling pathways displayed in the heatmap. Grey bars right of the heatmap show the total signaling strength of a pathway in all cell clusters. The relative signaling strength indicated by ranging color from white (low) to green (high). All cells included in these graphs originate from the plaque.

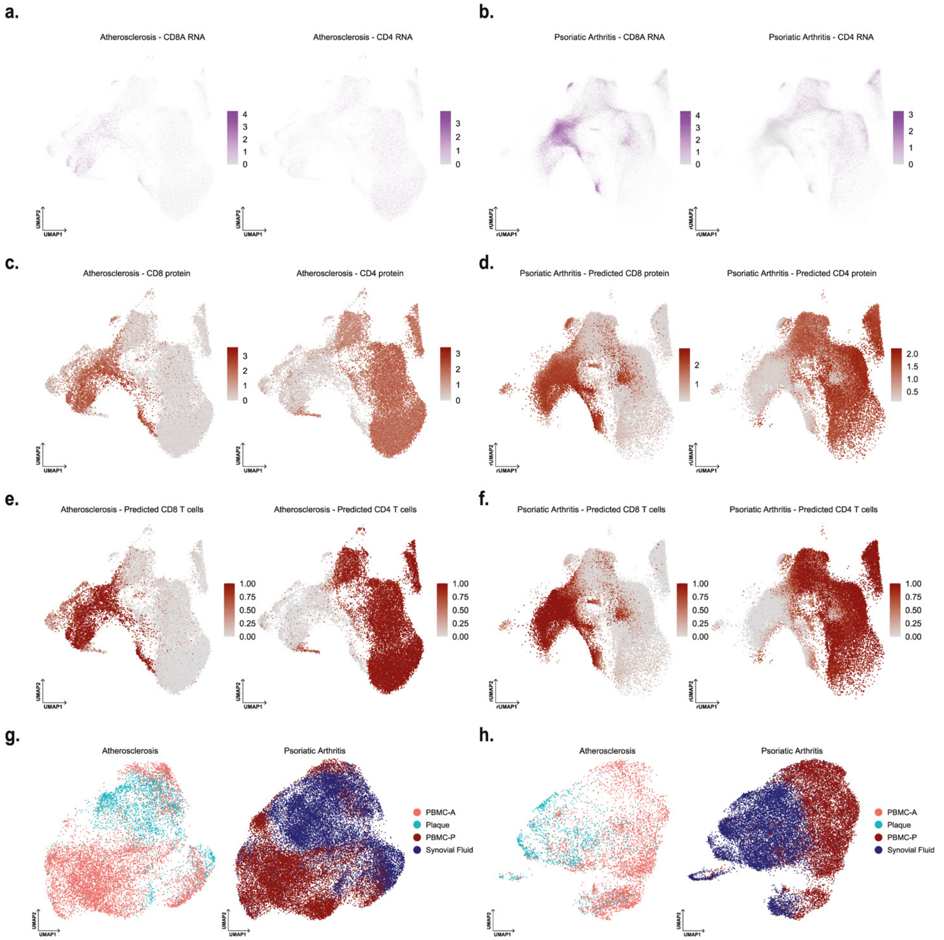

Extended Data Fig. 9. Projection of CD4$^+$ and CD8$^+$ T-cells of integrated atherosclerosis and psoriatic arthritis single-cell TCR sequencing data on the reference UMAP projection of CD4$^+$ and CD8$^+$ atherosclerosis data. a UMAP visualization of RNA expression of CD8A and CD4 on atherosclerosis T-cells. **b.** rUMAP visualization of RNA expression of CD8A and CD4 on psoriatic arthritis T-cells. **c.** UMAP visualization of protein expression of CD8 and CD4 on atherosclerosis T-cells. **d.** rUMAP visualization of predicted protein expression of CD8 and CD4 on psoriatic arthritis T-cells. **e.** UMAP visualization of selected CD8$^+$ and CD4$^+$ atherosclerosis T-cells. **f.** UMAP visualization of selected CD8$^+$ and CD4$^+$ psoriatic arthritis T-cells. **g.** UMAP of integrated CD4$^+$ T-cells split by diseased and grouped by tissue type. **h.** UMAP of integrated CD8$^+$ T-cells split by diseased and grouped by tissue type.

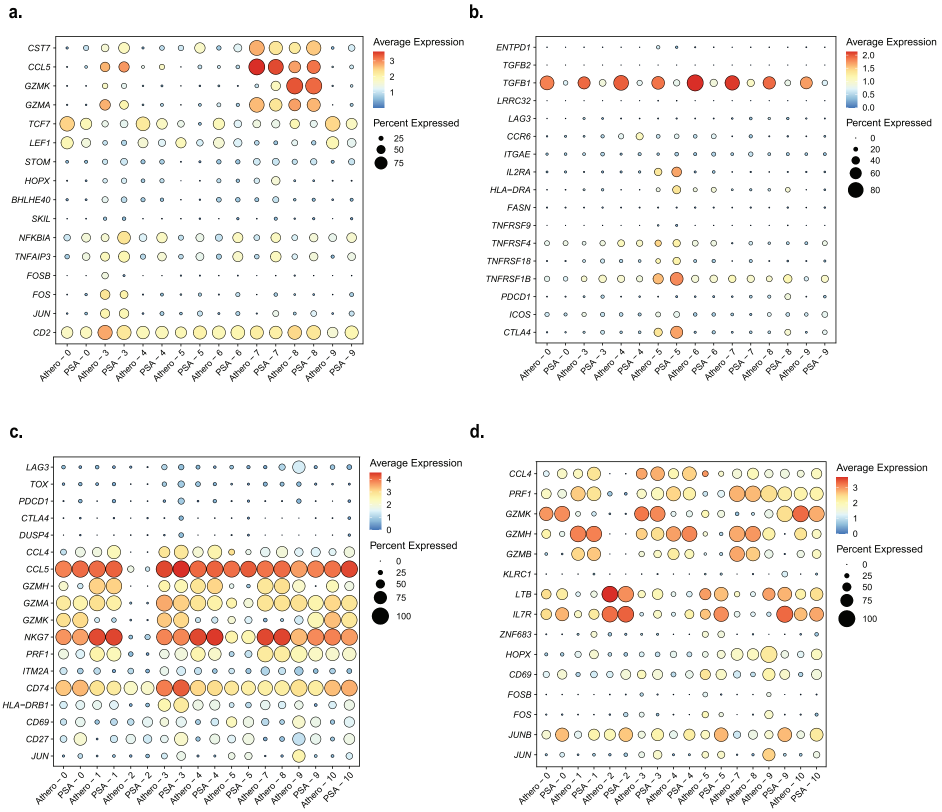

Extended Data Fig. 10. Extended dot plots with characterizing genes for atherosclerosis and psoriatic arthritis overlapping clonal expanded T-cells. Dotplots with genes used to characterize overlapping clusters of atherosclerosis and psoriatic arthritis per disease and per cluster of respectively CD4$^+$ cluster 3 genes(**a**), CD4$^+$ cluster 5 genes (**b**) CD8$^+$ cluster 3 genes(**c**) and CD8$^+$ cluster 5 genes (**d**).